HHS Public Access

Author manuscript

Immunity. Author manuscript; available in PMC 2019 July 17.

Published in final edited form as:

Immunity. 2018 July 17; 49(1): 93–106.e7. doi:10.1016/j.immuni.2018.05.004.

Sympathetic neuronal activation triggers myeloid progenitor proliferation and differentiation

Sathish Babu Vasamsetti[1,8], **Jonathan Florentin**[1,8], **Emilie Coppin**[1], **Lotte Stiekema**[2], **Kang H. Zheng**[2], **Muhammad Umer Nisar**[7], **John Sembrat**[1,3,4], **David Levinthal**[5], **Mauricio Rojas**[1,3,4,6], **Erik S. Stroes**[2], **Kang Kim**[1,7], and **Partha Dutta**[1,9,10,*]

[1]Pittsburgh Heart, Lung, Blood, and Vascular Medicine Institute, University of Pittsburgh, Pittsburgh, PA, USA [2]Department of Vascular Medicine, University of Amsterdam, Amsterdam, The Netherlands [3]Department of Medicine, Division of Pulmonary, Allergy, and Critical Care Medicine; University of Pittsburgh Medical Center; Pittsburgh, PA, USA [4]The Dorothy P. and Richard P. Simmons Center for Interstitial Lung Disease; University of Pittsburgh Medical Center; Pittsburgh, PA, USA [5]Division of Gastroenterology, Hepatology and Nutrition, Department of Medicine, University of Pittsburgh, Pittsburgh, PA, USA [6]McGowan Institute for Regenerative Medicine, University of Pittsburgh School of Medicine; Pittsburgh, PA, USA [7]Department of Bioengineering, University of Pittsburgh School of Engineering, Pittsburgh, PA, USA [8]Department of Immunology, University of Pittsburgh, Pittsburgh, PA, USA [9]Division of Cardiology, Department of Medicine, University of Pittsburgh, Pittsburgh, PA, USA

SUMMARY

There is a growing body of research on the neural control of immunity and inflammation. However, it is not known if the nervous system can regulate the production of inflammatory myeloid cells from hematopoietic progenitor cells in disease conditions. Myeloid cell numbers in diabetic patients were strongly correlated with plasma concentrations of norepinephrine, suggesting the role of sympathetic neuronal activation in myeloid cell production. The spleens of diabetic patients and mice contained higher number of tyrosine hydroxylase (TH)-expressing leukocytes that produced catecholamines. Granulocyte macrophage progenitors (GMP) expressed the β_2 adrenergic receptor, a target of catecholamines. Ablation of splenic sympathetic neuronal signaling using surgical, chemical and genetic approaches diminished GMP proliferation and

*Correspondence: duttapa@pitt.edu.

[8]Equally contributed to this work

[10]Lead Contact

Conflict of interest: The authors have declared that no conflict of interest exists.

AUTHOR CONTRIBUTIONS

SBV and JF were involved in conducting experiments, data analysis, and writing the manuscript. EC was involved in conducting experiments. MUN performed the ultrasound imaging experiment, and KK provided critical insight in ultrasound image analysis. LS, KHZ and ESS provided us with serum and blood leukocytes from patients. MR and JS provided us with spleen samples from deceased donors. DL provided us with insights in experiments involving splenic SNS. PD was involved in designing research studies, conducting experiments, acquiring and analyzing data, and writing the manuscript.

myeloid cell development. Finally, mice lacking TH-producing leukocytes had reduced GMP proliferation, resulting in diminished myelopoiesis. Taken together, our study demonstrates that catecholamines produced by leukocytes and sympathetic nerve termini promote GMP proliferation and myeloid cell development.

eTOC blurb

Neural control of immunity and inflammation has been reported. Vasamsetti and colleagues demonstrate that the sympathetic nervous system controls the development of inflammatory myeloid cells from their progenitors in inflammatory conditions.

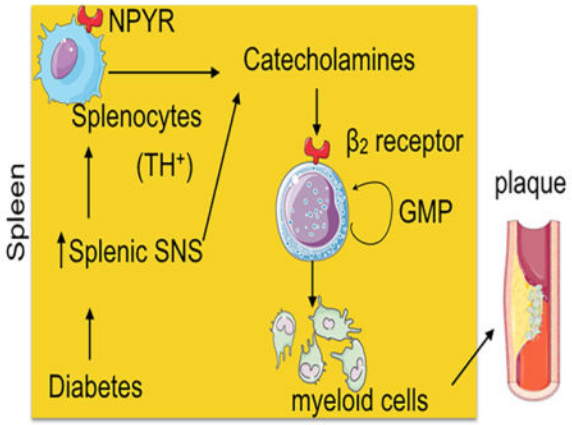

INTRODUCTION

Recent studies have shown that the immune system and the nervous system can communicate using common molecular signaling cues in various organ systems such as the central nervous system and the digestive system(Veiga-Fernandes and Pachnis, 2017). The myenteric plexus of the enteric nervous system contains macrophages and mast cells(Schemann and Camilleri, 2013), which are under neural control. Moreover, neuroimmune communication affects functions of an organ. For example, gut macrophage-derived bone morphogenesis protein 2 (BMP2) in response to enteric neuron signaling regulates gastrointestinal activity(Muller et al., 2014). Immune cells, such as macrophages and T cells, can produce catecholamines(Andersson and Tracey, 2012; Barnes et al., 2015; Brown et al., 2003; Jung et al., 2016; Laukova et al., 2013). Neural regulation of inflammation has been demonstrated by several studies(Andersson and Tracey, 2012). Vagus nerve stimulation dampens pro-inflammatory activity of macrophages(Wang et al., 2003), and vagotomy decreases group 3 innate lymphoid cell (ILC3) numbers(Dalli et al., 2017). Acetylcholine-producing T cells mediate anti-inflammatory responses after vagal nerve stimulation(Rosas-Ballina et al., 2011). Moreover, splenic sympathetic neuronal activation deploys T cells to the aorta and kidney, mediating hypertension(Carnevale et al., 2014; Tracey, 2014). Additionally, adrenergic signaling regulates hematopoietic stem cell mobilization(Scheiermann et al., 2012). Collectively, these studies suggest that the autonomic nervous system has promise as a therapeutic target to reduce inflammation in disease. As discussed above, most of the studies focused on the role of the autonomic

nervous system in inflammation. However, little is known about the involvement of the autonomic nervous system in inflammatory cell development in disease.

The aim of the present study is to understand the role of the sympathetic nervous system (SNS) in hematopoietic progenitor cell proliferation and their differentiation into inflammatory myeloid cells in disease. To investigate this, we used mouse models of type 1 and 2 diabetes since SNS activation in diabetes is well known(Esler et al., 2001; Seals and Bell, 2004; Thorp and Schlaich, 2015). We investigated the effect of SNS activation in splenic myeloid cell development because the spleen plays a pivotal role in emergency hematopoiesis in different diseases like myocardial infarction (MI) (Leuschner et al., 2012) and in cancer(Cortez-Retamozo et al., 2012). The spleen acts as a reservoir of inflammatory monocytes, which are released into the bloodstream and recruited to sites of inflammation(Swirski et al., 2009).

In the current study, we observed a previously unappreciated regulation of myelopoiesis by the SNS. We found that leukocyte, monocyte and inflammatory monocyte numbers in patients were strongly correlated with plasma concentration of norepinephrine (NE), suggesting the role of sympathetic neuronal activation in inflammatory myeloid cell production. We showed, in type 1 and 2 diabetes mouse models, elevated number of myeloid cells in the spleen and blood. Moreover, the spleens of diabetic mice harbored elevated numbers of highly proliferating granulocyte macrophage progenitors (GMP). Adoptive transfer of GMP in diabetic mice revealed that the progenitors gave rise to higher number of myeloid cells in the spleen. Splenic myeloid expansion was not secondary to the increased bone marrow (BM) hematopoietic progenitors and their subsequent mobilization to the spleen. Additionally, we observed that the spleen of diabetic mice had high SNS activity. Surgical and chemical denervation of splenic sympathetic neurons in diabetic mice demonstrated reduced GMP differentiation and decreased splenic myelopoiesis, whereas sympathetic neuronal ablation did not change BM myelopoiesis. Furthermore, we found that splenic GMP expressed high amounts of the β_2 adrenergic receptor. Selective β_2 blocker treatment in diabetic mice reduced splenic GMP proliferation and myeloid cell production. Diabetic mice harbored increased number of TH^+ leukocytes, which expressed high amounts of neuropeptide Y receptors, involved in neuroimmune signaling. Finally, diabetic mice lacking TH-producing leukocytes had reduced GMP proliferation and differentiation. This resulted in diminished splenic myelopoiesis. Altogether, these data indicate that elevated splenic sympathetic neuronal tone and paracrine activity of the catecholamines released by splenocytes in diabetes lead to GMP proliferation and differentiation into myeloid cells.

RESUTS

Inflammatory monocyte numbers correlate with plasma concentration of NE in patients

To investigate association between SNS activation and leukocytosis, we measured plasma NE and circulatory leukocyte contents in humans. We found that leukocyte, monocyte and inflammatory monocyte numbers strongly correlated with plasma NE concentrations (Figure 1A). Diabetic patients had higher plasma concentrations of NE than non-diabetic patients (Figure 1B), and plasma NE amounts correlated with glycosylated hemoglobin (Hba1c) quantities (Figure 1C). Additionally, we found that diabetic patients had elevated number of

leukocytes, monocytes and inflammatory monocytes compared to non-diabetic individuals (Figure 1D). Collectively, these data reveal a strong association between SNS activation and myeloid cell frequency. Since NE binds to the adrenergic receptors and mediate a cascade of cellular responses, we measured the expression of the adrenergic receptors on GMP, the immediate progenitors of myeloid cells. We found that human GMP expressed high amount of the β_2 adrenergic receptor (Figure 1E). Altogether, these data suggest a causative link between sympathetic neuronal activation and myeloid cell development.

Diabetes exaggerates splenic myelopoiesis

To investigate the role of SNS activation in myelopoiesis, we used mouse models of streptozotocin (stz)-mediated type 1 and high fat diet-induced type 2 diabetes. Since splenic myelopoiesis is important in pathogenesis of different diseases(Murphy et al., 2011; Robbins et al., 2012; Tall and Yvan-Charvet, 2015), we investigated splenic myelopoiesis in diabetic mice. We found that, at 1 month after stz treatment, mice had elevated numbers of different splenic myeloid cell subsets compared to non-diabetic control (Figure S1A). The elevated myeloid cell numbers persisted at 2 and 4 months after diabetes induction. Confocal imaging of splenic sections confirmed the increased frequency of $CD11b^+$ myeloid cells in diabetic mice (Figure S1B).

Myeloid cells produced in the spleen in disease conditions egress into the blood and infiltrate inflamed organs(Leuschner et al., 2012; Swirski et al., 2009). To check this phenomenon in diabetes, we enumerated different myeloid cell subsets in blood. We found increases in number and frequency of these cells in blood circulation 1, 2 and 4 months after stz injection (Figures S1C and S1D). In contrast, the frequencies of B and T lymphocytes in the blood were unaltered in diabetic mice (Figure S1E).

Splenic granulocyte macrophage progenitors (GMP) are activated in diabetic mice

Activation and proliferation of GMP have been reported in cardiovascular disease such as atherosclerosis(Westerterp et al., 2012) and MI (Dutta et al., 2015). Activated GMP differentiate into myeloid cells, which are mobilized to sites of inflammation. To investigate the source of myeloid cells in diabetes, we enumerated GMP in the spleen of diabetic mice. We found about 2-fold increase in GMP numbers in the spleen of diabetic mice (Figure 2A), indicating a higher proliferation rate of the progenitors in diabetes. To test GMP proliferation in diabetic mice, we used BrdU, which can be incorporated into the DNA strand during the S phase of the cell cycle. After 2 weeks of BrdU pulse (Figure 2B), we found that most of the splenic progenitors were $BrdU^+$ (Figure S1F). The dilution of BrdU in the progenitor cells of diabetic mice was higher than non-diabetic control mice (Figure 2B), suggesting that the splenic progenitor cells proliferated highly in diabetic mice. Additionally, genes involved in cell cycle progression, such as cyclins (*Ccnb1, Ccnd1* and *Ccne2*) and cyclin-dependent kinases (*Cdk2, 3*, *4* and *6*) were enriched in splenic GMP of diabetic mice (Figure 2C). Altogether, these data indicate that diabetes drives splenic GMP into the cell cycle.

Highly proliferative GMP in the spleen of diabetic mice can differentiate into myeloid cells(Herault et al., 2017). To ascertain differentiation ability of splenic GMP in diabetic

mice, we isolated the progenitor cells from GFP^+ mice and injected into either diabetic or non-diabetic mice (Figure 2D). We found that the donor-derived GMP generated higher number of myeloid cells in the spleen of diabetic mice. Confocal microscopy of the spleen revealed GMP transferred into diabetic mice produced higher number of progenies and clusters compared to non-diabetic control mice, indicating the active proliferation and differentiation of GMP in diabetes(Herault et al., 2017) (Figure 2E). Next, we investigated if the splenic progenitors isolated from diabetic mice retain higher proliferation ability in non-diabetic mice. Towards this end, we isolated GMP from congenically different diabetic and non-diabetic control mice and co-transferred them in sub-lethally irradiated GFP^+ non-diabetic mice (Figure 2F). Two weeks after the transfer, we found that GMP-derived from diabetic donors produced higher proportion of myeloid cells in the spleen. Taken together, these data suggest that splenic GMP in diabetic mice have higher proliferation and differentiation ability.

Splenic GMP differentiation and myelopoiesis in diabetes are regulated by sympathetic neuronal activity

High sympathetic neuronal activity in the BM of diabetic mice(Ferraro et al., 2011) and humans(Esler et al., 2001; Seals and Bell, 2004; Thorp and Schlaich, 2015) has been reported. To investigate sympathetic neuronal activity in the spleen in diabetes, we stained spleen sections for tyrosine hydroxylase (TH), a rate limiting enzyme in catecholamine synthesis. We found increased number of TH-expressing splenocytes in diabetic mice (Figure 3A) and patients (Figure 3B). Confocal microscopy of the spleen after GFP^+ GMP transfer revealed that GMP formed clusters near TH-expressing cells in diabetic mice (Figure 3C, Supplementary Movie 1 and Supplementary Movie 2). In fact, about 30% of GFP^+ cells derived from the transferred GMP were within <1 μm distance from TH^+ splenocytes. To investigate the effect of sympathetic neuronal activation on splenic myelopoiesis in diabetic mice, we performed sympathetic neuronal ablation with 6-hydroxydopamine (6-OHDA). 6-OHDA treatment reduced TH-producing splenocytes (Figure 3D). Concomitantly, the spleens of diabetic mice after 6-OHDA treatment contained about 2-fold reduced myeloid cells and monocytes compared to PBS-treated control (Figure 3E). Four days after adoptive transfer of GMP, the spleens of 6-OHDA-treated mice had fewer GFP^+ myeloid cells than PBS-treated mice (Figure 3F). Confocal microscopy of the spleen demonstrated similar reduction of GFP^+ cell numbers and clusters after 6-OHDA treatment (Figure 3G, Supplementary Movie 2 and Supplementary Movie 3). Collectively, these data indicate that higher activity of sympathetic neurons in the spleen of diabetic mice induces GMP differentiation into myeloid cells.

Hyperglycemia induces myelopoiesis and TH expression in splenic leukocytes

Next we investigated the mechanisms of myelopoiesis in diabetic mice. Because type 1 diabetic mice have reduced insulin and high blood glucose concentrations, we assessed if hyperglycemia in these mice triggers myeloid cell development. To this end, we injected the mice with phlorizin, an inhibitor of sodium-glucose co-transporters (SGLT). This treatment reduced the fasting blood glucose concentrations (Figure 3H). Concomitantly, splenic GMP proliferation (Figure 3I) and myeloid cell number (Figure 3J) were diminished. Furthermore, the spleens of diabetic mice treated with phlorizin contained fewer TH-expressing

splenocytes (Figure 3K). In aggregate, these data indicate that hyperglycemia induces myelopoiesis and TH expression in splenocytes of diabetic mice.

β_2 adrenergic receptor blockade reduces splenic GMP proliferation and myelopoiesis

Since spleens of diabetic mice harbored increased number of TH^+ splenocytes, we investigated cellular sources of TH. We observed that TH^+ cells were $CD45^+$, confirming that they are leukocytes (Figure S2A). As expected, splenic nerves ($PGP9.5^+$) also expressed TH. Lymphocytes, neutrophils and macrophages sorted from spleens of diabetic mice (Figure 4A) and humans (Figures 4B & S2B) expressed TH mRNA. Consistently, confocal microscopy of splenic sections of diabetic mice (Figure 4C) and humans (Figure 4D) showed that these splenocytes produced TH protein. Spleens of diabetic mice harbored higher proportions of TH-expressing T cells, macrophages and neutrophils. To further confirm that leukocytes produce TH, we generated a reporter mouse (TH-tdTomato) that express tdTomato in TH-expressing cells. We checked tdTomato expression in splenic leukocytes using flow cytometry (Figures 4E & S3A) and confocal microscopy (Figure S3B). We observed that B lymphocytes and macrophages were the most abundant TH-expressing cells in the spleen. We also confirmed TH expression in isolated splenic leukocytes by immuno blot (Figure 4F). Consistent with low TH mRNA expression (Figure 4A & 4B), splenic monocytes did not express TH protein (Figure S3C). To determine if monocytes express TH after they differentiate into macrophages, we differentiated THP-1 cells, a human monocyte cell line. After differentiating into macrophages, these cells elevated *Th* expression (Figure S3D). Consistent to their TH expression, macrophages produced NE and epinephrine (Figure 4G). The production of the catecholamines increased in presence of IL-4, consistent with a previous finding(Nguyen et al., 2011). Flow cytometry (Figure 4H & S3E) and confocal imaging (Figure 4I, S3F, and Supplementary Movie 4 & 5) confirmed that the spleens of diabetic mice harbored elevated numbers of $tdTomato^+$ leukocytes, B cells, macrophages, neutrophils and T cells.

The catecholamines bind to the adrenergic receptors and mediate a cascade of cellular responses. BM multipotent progenitors express adrenergic receptors(Muthu et al., 2007). Similarly, we found that splenic GMP and other hematopoietic progenitors in mice expressed high amounts of the β_2 adrenergic receptor (Figure 4J), which is consistent with high expression of this adrenergic receptor in human GMP (Figure 1E). A specific β_2 blocker treatment reduced myeloid cell numbers in the blood and spleen (Figures 4K & 4L). Consistently, the treatment lowered splenic GMP proliferation (Figure 4M). Taken together, these data indicate that β_2 adrenergic receptor signaling mediates splenic GMP proliferation and their differentiation into myeloid cells.

Sympathetic neuronal regulation of myelopoiesis in type 2 diabetic mice

We found about 2-fold increase in splenic myeloid cell, monocyte and Ly-$6C^{hi}$ monocyte content after feeding C57BL/6 mice with a high fat diet for 16 weeks (Figure 5A), similar to type 1 diabetic mice. These diabetic mice had increased number of highly proliferative splenic GMP (Figures 5B & 5C). Additionally, spleens harbored higher number of TH^+ leukocytes, macrophages and T cells (Figure 5D). Finally, to investigate the role of adrenergic signaling in myelopoiesis in type 2 diabetes, we adoptively transferred DiO-

labeled GMP from β_1 and β_2 adrenergic receptor-deficient (*Adrb1*$^{-/-}$ and *Adrb2*$^{-/-}$) or wild type mice into diabetic mice. Four days after the adoptive transfer, we found that GMP isolated from *Adrb1*$^{-/-}$ and *Adrb2*$^{-/-}$ diabetic mice produced lower number of myeloid cells in the spleen (Figure 5E). Collectively, these data show that myelopoiesis in type 2 diabetic mice is dependent on local splenic catecholamine exposure.

Splenic sympathectomy reduces GMP proliferation and diminishes myelopoiesis

Our data indicated that SNS activation in diabetes increased splenic myelopoiesis. To investigate if this effect is specific to splenic sympathetic neuronal activation, we performed surgical splenic sympathectomy in diabetic mice. Splenic sympathectomy reduced PGP9.5$^+$ nerve fibers in the spleen (Figure 6A), indicating successful denervation. Moreover, the surgery reduced TH$^+$ splenic leukocyte numbers and also diminished GMP proportions and numbers (Figure 6A & 6B). Furthermore, the mice with splenic sympathectomy had lower percentage of GMP in the S-G2-M phases (proliferating cells) and higher percentage of GMP in the G0 phase (quiescent cells) of the cell cycle (Figure 6C & 6D). In contrast, GMP number (Figure S4A) and proliferation (Figure S4B) in the BM did not alter after splenic sympathectomy. Moreover, splenic sympathectomy reduced splenic monocyte numbers (Figure S4C); however, the surgery did not change myeloid cell content in the BM (Figure S4D), indicating the organ-specific effect after splenic sympathectomy. Consistent with diminished splenic GMP number and proliferation, the spleen (Figure 6E) and blood (Figure 6F) contained declined number of CD11b$^+$ myeloid cells and monocytes, respectively, after splenic sympathectomy.

TH$^+$ leukocytes are equipped with receptors involved in neuroimmune signaling

After splenic sympathectomy, we observed reduction in TH expression in leukocytes (Figure 6A). This suggests a feed forward loop of adrenergic signaling from nerves to TH-expressing hematopoietic cells. To investigate this more carefully, we determined the distance of TH$^+$ and TH$^-$ splenic leukocytes from splenic nerves. About 40% of TH$^+$ and only 15% of TH$^-$ leukocytes were within 1 μm distance from splenic nerves (Figure S4E & S4F), indicating their direct contact. We generated mice that express diphtheria toxin receptor (DTR) under *Th* promoter in neurons by transplanting wild type BM cells in lethally irradiated *Th*-cre-ROSA-iDTR mice. We induced diabetes in these mice and administered DT locally in the spleen using micro-osmotic pumps. DT administration reduced nerve fibers and TH-expressing leukocytes in the spleen (Figure 6G). Collectively, these data indicate a feed forward loop of adrenergic signaling from nerves to TH-expressing hematopoietic cells. To determine if TH$^+$ leukocytes are more effective in neuroimmune communication than the TH$^-$ leukocytes, we sorted these cells from the spleens of non-diabetic and diabetic *Th*-tdTomato mice. We observed that TH$^+$ leukocytes isolated from diabetic mice had higher expression of the receptors for neuropeptide (NP) Y4, Y5 and Y6, involved in neuroimmune communication(Straub et al., 2000), compared to TH$^-$ leukocytes (Figure 6H). Furthermore, TH$^+$ cells had elevated expression of *Npy4r*, *Npy5r* and *Npy6r* in diabetic mice compared to non-diabetic mice. These data suggest that NPY produced by splenic sympathetic nerve termini mediate nerve to TH$^+$ leukocyte communication in diabetes.

TH^+ leukocytes mediate myelopoiesis

We found that TH^+ leukocytes are in close contact with GMP clusters, suggesting the role of TH^+ leukocytes in myeloid cell production. To test this, we generated mice that express the DTR under *Th* promoter in hematopoietic cells (Figure S4G). We found that TH^+ leukocyte depletion with DT (Figure 6I) resulted in reduced myeloid progenitor and GMP numbers (Figure 6J), and diminished myeloid cell and monocyte contents in the spleen and blood (Figure S4H and S4I). Next, we investigated if splenic nerves are important for myelopoiesis in diabetes. To accomplish this, we used mice expressing DTR under *Th* promoter in neurons. Depletion of splenic nerves by local administration of DT using micro-osmotic pumps in these mice resulted in diminished myeloid cell and monocyte numbers in the spleen (Figure S4J) and GMP proliferation (Figure S4K).

Ablation of sympathetic neuronal activity ameliorates diabetes complication

The major cause of death of diabetic patients is cardiovascular disease, such as atherosclerosis (Howard and Wylie-Rosett, 2002; Wendt et al., 2002), which is a complication of diabetes. To investigate this, we induced diabetes in atherosclerotic $Apoe^{-/-}$ mice with stz injection. Consistent to reported insidious role of myeloid cells in plaque progression and rupture(Libby, 2012, 2013; Libby et al., 2011), we found highly inflamed (Figures S5A & S5B) and vulnerable (Figure S5C) plaques in diabetic $Apoe^{-/-}$ mice. These findings complemented previously published data on plaque macrophages in diabetic mice(Johansson et al., 2008; Kanter et al., 2012; Parathath et al., 2011).

Additionally, we found that the diabetic $Apoe^{-/-}$ mice had increased numbers of myeloid cells, monocytes, Ly-$6C^{hi}$ monocytes and neutrophils in the spleen and blood (Figure S6A & S6B). The mice also had increased GMP numbers in the spleen (Figure S6C), suggesting the role of splenic hematopoiesis in diabetes-associated atherosclerosis. In line with this, splenectomy in diabetic $Apoe^{-/-}$ mice reduced myeloid cell and inflammatory monocyte numbers in the aorta (Figure S6D), resulting in reduced atherosclerotic plaque areas and thicker fibrous caps (Figure S6E).

Splenic myelopoiesis has been shown to increase inflammation and vulnerability of atherosclerotic plaques(Swirski et al., 2007; Tall and Yvan-Charvet, 2015). Since we found sympathetic neuronal ablation with 6-OHDA decreased splenic myelopoiesis in diabetic mice (Figure 3), we investigated if 6-OHDA treatment could diminish inflammation in atherosclerotic lesions of diabetic mice. We found reduced splenic myeloid cell and monocyte numbers in 6-OHDA-treated mice (Figures 7A, S7A & S7B), confirming that sympathetic neuronal ablation curbs diabetes-induced splenic myelopoiesis. Next, we enumerated myeloid cells in the aortas of $Apoe^{-/-}$ mice (Figures 7B, S7C & S7D). We observed declined number of myeloid cells and inflammatory monocytes in the aortas of $Apoe^{-/-}$ mice after sympathetic neuronal ablation. Masson's trichrome staining of aortic root sections demonstrated smaller plaque size and thicker fibrous caps in diabetic mice after the chemical sympathectic blockade (Figure 7C & S7E). To measure plaque area *in vivo*, we performed ultrasound imaging and found reduced plaque area in 6-OHDA-injected diabetic $Apoe^{-/-}$ mice (Figure 7D). Altogether, these results indicate that sympathetic neuronal blockade in diabetic mice improves the features of stable atherosclerotic lesions.

Because splenic sympathectomy reduced myeloipoiesis in diabetic mice (Figure 6) and myeloid cells generated in the spleen aggravates atherosclerosis pathogenesis(Swirski et al., 2007; Tall and Yvan-Charvet, 2015), we investigated the effect of splenic sympathectomy in atherosclerosis. We found that aortas of diabetic *Apoe*$^{-/-}$ mice, after splenic sympathectomy, had reduced amounts of mRNA of monocyte chemoattractant protein-1 (Figure 7E), responsible for myeloid cell infiltration into atherosclerotic lesions. In line with this finding, we observed lower number of myeloid cells in the aortas of splenic sympathectomized mice (Figure 7F). Since splenic myelopoiesis augments inflammation and vulnerability of atherosclerotic plaques(Swirski et al., 2007; Tall and Yvan-Charvet, 2015), we checked the features of plaque vulnerability, such as plaque area and fibrous cap thickness and found that surgical denervation of splenic sympathetic neurons reduced plaque area and increased fibrous cap thickness (Figures 7G & S7F).

Next, we determined the contribution of spleen in supplying inflammatory myeloid cells to atherosclerotic plaques. Three weeks after spleen transplantation, myeloid cell enumeration revealed an increase in number of donor-derived myeloid cells, monocytes and neutrophils in the aorta and blood of diabetic recipient mice (Figure S7G). Because the egress of monocytes from the spleen depends on angiotensin 2(Swirski et al., 2009), we delivered an angiotensin converting enzyme (ACE) inhibitor into the spleen of diabetic *Apoe*$^{-/-}$ mice using micro-osmotic pumps for 3 weeks. ACE inhibitor treatment increased monocyte numbers in the spleen, whereas macrophage numbers in the aorta decreased (Figures 7H & S7H), indicating their reduced egress from the spleen. These mice also had thicker fibrous caps of atherosclerotic lesions compared to the control group (Figure 7I). To ascertain the effect of NE on splenic myelopoiesis, we exogenously administered NE in diabetic *Apoe*$^{-/-}$ mice using micro-osmotic pumps. The treatment resulted in elevated GMP and myeloid cell numbers in the spleen (Figure 7J) but not in the BM (Figure 7K). We further observed increased macrophages in the aorta (Figure 7L) and thinner fibrous cap in atherosclerotic plaques (Figures 7M & S7I) compared to the vehicle-treated group.

To determine the role of catecholamines secreted by splenic nerves in myelopoiesis and atherosclerosis, we injected diabetic *Apoe*$^{-/-}$ mice with reserpine in the spleen using micro-osmotic pumps. Reserpine blocks the uptake of catecholamines into synaptic vesicles by inhibiting the vesicular monoamine transporter 2(Rosas-Ballina et al., 2008). However, it did not reduce catecholamine secretion by leukocytes in culture (Figure S7J). In contrast to this finding, reserpine not only reduced catecholamine production by splenic nerve fibers but also by splenic leukocytes *in vivo* (Figure S7K), indicating a crosstalk between splenic nerves and leukocytes. Reserpine treatment reduced splenic myelopoiesis (Figures 7N & 7O). Concomitantly, atherosclerotic plaque burden decreased, and fibrous cap thickness increased in these mice compared to PBS-injected group (Figure 7P). These data indicate that catecholamines secreted by splenic nerve termini and leukocytes are important for myelopoiesis and atherosclerosis.

Collectively, these data indicate that splenic sympathetic neuronal activation in diabetes-associated atherosclerosis amplifies inflammatory myeloid cell production by increasing GMP proliferation and differentiation. These newly produced inflammatory myeloid cells in

the spleen infiltrate into atherosclerotic plaques and increase the features of plaque vulnerability.

BM does not contribute to splenic myeloid expansion in diabetes

Consistent with a published report(Nagareddy et al., 2013), we found that the BM of diabetic mice harbored higher numbers of myeloid cell subsets compared to non-diabetic mice (Figure S7L). However, we did not observe any difference in the number of TH^+ cells in BM between these two groups (Figure S7M). Consistently, systemic DT administration in mice expressing iDTR in TH^+ hematopoietic cells (Figure S7N) and β_2 blocker treatment (Figure S7O) did not alter myeloid progenitor and GMP numbers in the femur. In aggregate, these data indicate that increased BM myelopoiesis in diabetic mice is not due to augmented sympathetic neuronal activity.

To assess if splenic myeloid expansion is secondary to BM myelopoiesis, we enumerated HSPC and GMP in the blood of diabetic mice. We did not observe an increase in the number of these progenitor populations in the blood of diabetic mice compared to non-diabetic mice (Figure 7Q), with is consistent to a recent finding (Ferraro et al., 2011). To address definitively if BM hematopoietic progenitors mobilize to the spleen in diabetic mice, we generated KikGR transgenic mice that express a Kikume Green-Red photoconvertible fluorescent protein under the control of a chicken beta actin promoter. Lin^- $C\text{-}kit^+$ progenitor cells isolated from these mice were adoptively transferred in non-diabetic and diabetic wild type mice. Four days after the transfer, the GFP^+ donor cells in the calvarium were photoconverted using an intravital microcope (Figure 7R). After photoconversion, GFP in these cells changed to RFP. Seven days after the photoconversion, we assessed the number of photoconverted (RFP^+) cells in the spleen to determine mobilization of these cells from the BM to the spleen. We did not find an increase in photoconverted cell numbers in the spleen of diabetic mice (Figure 7S). The spleens of diabetic mice contained less number of photoconverted cells although this decrease in cell number did not reach statistical significance, supporting the finding that diabetic patients have impaired mobilization of hematopoietic progenitors from the BM (Ferraro et al., 2011). Altogether, these data indicate that diabetes does not induce mobilization of BM hematopoietic progenitor cells to the spleen; rather splenic hematopoietic progenitors proliferate and differentiate into myeloid cells.

DISCUSSION

Sympathetic neuronal activation in diabetes is well known(Esler et al., 2001; Seals and Bell, 2004; Thorp and Schlaich, 2015). We found a significant correlation between plasma concentration of catecholamines and circulatory leukocyte counts in patients, suggesting the role of SNS activation in leukocyte production. The effect of the SNS and catecholamine signaling on GMP proliferation and their differentiation into myeloid cells had not been studied. We serendipitously found higher number of TH^+ cells in the spleens of diabetic patients and mice. Reduced GMP proliferation and differentiation in diabetic mice after splenic sympathectomy indicates that higher sympathetic neuronal tone induces GMP proliferation. Additionally, sympathectomized spleen harbored reduced number of TH^+

cells. Mice lacking TH^+ cells exhibited reduced GMP proliferation and myelopoiesis. These observations indicate that diabetic mice have elevated sympathetic neuronal tone, which results in additional catecholamine production by splenic leukocytes. The data presented in the study indicate that both splenic nerve and TH^+ leukocytes are crucial to splenic myelopoiesis. Furthermore, the experiment using reserpine to block postsynaptic release of catecholamines also reduced catecholamine production by leukocytes, indicating that catecholamines produced by splenic nerve termini trigger catecholamine production by leukocytes. In line with this, we found sympathetic neuronal denervation and DT-mediated depletion of splenic nerves resulted in declined frequency of TH^+ leukocytes in the spleen. Because catecholamine production by leukocytes depends on splenic neurons, determining the specific roles of catecholamines produced by these two cell types is beyond the scope of this study. Additionally, we observed that TH^+ leukocytes were located close to splenic nerves and had higher expression of neuropeptide Y receptors, which are involved in neuroimmune communication. Future mechanistic studies are required to determine if the expression of these receptors in TH^+ cells is crucial to splenic myelopoiesis in diabetes.

Splenic emergency myelopoiesis has been studied in different diseases such as cancer(Cortez-Retamozo et al., 2012), hyperlipidemia(Robbins et al., 2012) and MI (Leuschner et al., 2012; Swirski et al., 2009). Myelopoiesis in the spleen maintains a steady flow of myeloid cells to sites of inflammation, such as atherosclerotic plaques and infarcted myocardium. Given that these cells play a critical role in tissue repair after a sterile injury and splenic monocytes exhibit a more vigorous inflammatory gene signature than BM monocytes(Dutta et al., 2012), it is imperative to know the mechanisms of splenic myelopoiesis.

The major cause of death of diabetic patients is cardiovascular complications(Howard and Wylie-Rosett, 2002; Wendt et al., 2002), primarily MI due to atherosclerotic plaque rupture. Diabetes can exacerbate pre-existing atherosclerosis by increasing plaque size and intralesional hemorrhage(Renard et al., 2004). Moreover, induction of diabetes in mice with established atherosclerosis causes plaque disruption in the brachiocephalic artery(Johansson et al., 2008). Consistently, we found that atherosclerotic plaques of diabetic mice had thinner fibrous caps, a feature of plaque vulnerability. Vulnerable atherosclerotic plaques in diabetic mice harbor highly proliferative and inflammatory macrophages(Kanter et al., 2012), which is in line with our data showing high number of plaque-dwelling myeloid cells. Although the contribution of plaque macrophages in diabetes-induced exacerbation of atherosclerosis is well accepted, the source of myeloid cells is not clear. Our data suggest that the splenic myelopoiesis is one of the sources of plaque macrophages in diabetic mice. Of note, plaque macrophages can also be derived from aortic smooth muscle cells(Shankman et al., 2015). The role of smooth muscle cell-derived macrophages in diabetic atherosclerosis is currently unknown. We found that splenic myelopoiesis is regulated by sympathetic neuronal activation in diabetes, whereas augmented sympathetic neuronal tone in diabetes does not induce BM myelopoiesis. Future studies are warranted to investigate the mechanisms of BM myelooiesis in diabetes.

The present study has identified multiple therapeutic targets, such as splenic sympathetic nerve and the β_2 adrenergic receptor on GMP, to curtail the production of inflammatory cells

in diabetes. β_1 blockers, such as metoprolol and carvedilol, are used in diabetic patients with hypertension. The effect of β_1 blockers in hyperglycemia is controversial. Most studies showed that the treatment does not alter insulin sensitivity in diabetic patients(Bokhari et al., 2014; Ostman, 1983). In contrast, carvedilol treatment was shown to reduce new onset of diabetes(DiNicolantonio et al., 2015). In the present study, we have reduced splenic GMP proliferation and inflammatory myeloid cell generation with a selective β_2 blocker and genetic deficiency of the adrenergic receptor β_2. We recognize the possibility of off-target effects of these methods. Generation of mice lacking the β_2 adrenergic receptor on GMP will help overcome this shortcoming.

Obesity and type 2 diabetes affect the function of hematopoietic stem(Nagareddy et al., 2014; Nagareddy et al., 2013; Orlandi et al., 2010; Trottier et al., 2012) and niche cells(Ferraro et al., 2011; Spinetti et al., 2013) in the BM. Our study focused on splenic myelopoiesis in the context of diabetes. The effect of the SNS on BM myelopoiesis remains to be investigated. Furthermore, the molecular mechanisms leading to sympathetic neuronal activation in diabetes remain to be explored. We found that GMP isolated from diabetic mice, when transferred into non-diabetic mice, can still proliferate and differentiate at a higher rate, indicating epigenetic changes of the progenitors in hyperglycemic environment. Future studies are required to identify the epigenetic marking responsible for continued proliferation and differentiation of GMP in normoglycemic environment.

STAR Methods

Key Resources Table

Reagent or resource	Source	Identifier
Chemicals		
42% Kcal% high fat diet for *Apoe*$^{-/-}$	Research Diets Inc	TD88137
6-Hydroxydopamine hydrobromide (6-OHDA)	Sigma-Aldrich	H116
60% Kcal% high fat diet	Research Diets Inc	D12492
AEC substrate	ScyTek	ACJ500
Bovine growth serum	Fisher Scientifics	SH3054103
Bovine serum albumin	Fisher Scientifics	BP1600-1
BrdU APC flow kit	BD Biosciences	552598
Captopril	Alfa Aesar	J63593
cDNA synthesis kit	Applied Biosystems	4387406
Cell Strainer	Fisher Scientifics	22363548
Collagenase-1	Sigma-Aldrich	C00130
Collagenase-IX	Sigma-Aldrich	C7657
Diphtheria Toxin	Sigma-Aldrich	D0654
Dio	Invitrogen	V22886
Dream Taq PCR Master mix (2X)	Thermo Scientific	K1071
EasySep mouse biotin positive selection kit	Stem Cell Technologies	18556

Reagent or resource	Source	Identifier
Epinephrine/norepinephrine ELISA kit	Abnova	KA1877
Fixation buffer for nuclear staining	BD biosciences	554655
Glucose test strips	Fisher Scientific	23111276
Glycoxylic acid monohydrate	Acros Organics	120170250
Hyalouronidase	Sigma-Aldrich	H35006
ICI 118,551	Sigma-Aldrich	I127
Immuno-blot HRP substrate	Millipore	WBLUR0500
L-Glutamine	Gibco	25030-081
Laemmli SDS sample buffer, reducing (6X)	Alfa Aesar	J61337
Micro-osmotic pumps	Alzet	Model 1002
MEM non-essential amino acids	Gibco	11140-050
Monobasic potassium phosphate	Acros Organics	212595000
Norepinephrine	Sigma-Aldrich	A7256
Penicillin-streptomycin mixture	Fisher Scientifics	ICN1670249
Permeabilization buffer for nuclear staining	BD Biosciences	558050
Phlorizin dihydrate	Sigma-Aldrich	P3449
Picopure TM RNA isolation kit	Applied Biosystems	1220401
RBC lysis buffer	Biolegend	420301
Recombinant IL-4	R&D	204-IL
Reserpine	Alfa Aesar	L03506
RIPA buffer	Alfa Aesar	J63324
RPMI 1640 medium	HyClone	SH30027LS
Sodium citrate	Fisher Scientifics	BP327
Streptozotocin	Sigma-Aldrich	S0130
SYBR green PCR master mix	Applied Biosystems	A25776
TRIzol	Fisher Scientifics	NC9574779
Vectastain ABC-HRP kit	Vector Laboratories	PK6100
Vector shield mounting medium with DAPI	Vector Laboratories	H1200
Primers		
Human ADRA1B-F CTTTCACGAGGACACCCTTAGC ADRA1B-R GCCCAACGTCTTAGCTGCTT	IDT	
Human ADRA2A-F TCGTCATCATCGCCGTGTTC ADRA2A-R AAGCCTTGCCGAAGTACCAG	IDT	
Human ADRB1-F ATCGAGACCCTGTGTGTCATT ADRB1-R GTAGAAGGAGACTACGGACGAG	IDT	
Human ADRB2-FTTGCTGGCACCCAATAGAAGC ADRB2-R CAGACGCTCGAACTTGGCA	IDT	
Human ADRB3-F GACCAACGTGTTCGTGACTTC ADRB3-R GCACAGGGTTTCGATGCTG	IDT	
Human β actin-F CATGTACGTTGCTATCCAGGC β actin-R CTCCTTAATGTCACGCACGAT	IDT	
Human TH-F GCTGGACAAGTGTCATCACCTG	IDT	

Reagent or resource	Source	Identifier
TH-R CCTGTACTGGAAGGCGATCTCA		
Mouse *Adra1b*- F CGGACGCCAACCAACTACTT *Adra1b*- R AACACAGGACATCAACCGCTG	IDT	
Mouse *Adra2a*- F GTGACACTGACGCTGGTTTG *Adra2a*- R CCAGTAACCCATAACCTCGTTG	IDT	
Mouse *Adrb1*- F CTCATCGTGGTGGGTAACGTG *Adrb1*- R ACACACAGCACATCTACCGAA	IDT	
Mouse *Adrb2*- F GGGAACGACAGCGACTTCTT *Adrb2*- R GCCAGGACGATAACCGACAT	IDT	
Mouse *Adrb3*- F GGCCCTCTCTAGTTCCCAG *Adrb3*- R TAGCCATCAAACCTGTTGAGC	IDT	
Mouse *Ccnb1*	Taqman	Mm03055893_gH
Mouse *Ccnd1*	Taqman	Mm00432359_m1
Mouse *Ccne2*	Taqman	Mm00438077_m1
Mouse *Cdk2*	Taqman	Mm00443947_m1
Mouse *Cdk3*	Taqman	Mm00518387_m1
Mouse *Cdk4*	Taqman	Mm00726334_s1
Mouse *Cdk6*	Taqman	Mm01311342_m1
Mouse *Gapdh*-F AGGTCGGTGTGAACGGATTTG *Gapdh*-R TGTAGACCATGTAGTTGAGGTCA	IDT	
Mouse *Mcp-1* F GTCCCTGTCATGCTTCTGG *Mcp-1*R GCTCTCCAGCCTACTCATTG	IDT	
Mouse *Th*-F GGCTTCTCTGACCAGGCGTAT *Th*-R TGCTTGTATTGGAAGGCAATCTC	IDT	
Flow cytometry Antibodies		
Human CD11C, BV650, APC	BD Biosciences	563403, 559877
Human CD123, BUV395, BV605	BD Biosciences	564195, 564197
Human CD14-biotin	Biolegend	325624
Human CD14, APC, APC-Cy7	BD Biosciences	555399, 557831
Human CD16, APC H7, BV711	BD Biosciences	560715, 563127
Human CD169 (siglec-1), PE	BD Biosciences	565248
Human CD2-biotin	BD Biosciences	555325
Human CD206, PE-CF594, FITC	BD Biosciences	564063,551135
Human CD24, PerCP-Cy5.5	BD Biosciences	561647
Human CD3-biotin	BD Biosciences	555338
Human CD3, BV510	BD Biosciences	563109
Human CD4-biotin	BD Biosciences	555345
Human CD45, AF700	BD Biosciences	560566
Human CD56, BV421	BD Biosciences	562751
Human CD8-biotin	BD Biosciences	555365
Human HLA-DR, APC-R700	BD Biosciences	565127
Mouse CD 115, PerCP-Cy5.5	eBioscience	46-1152-82
Mouse CD 34, FITC	BD Biosciences	553733

Reagent or resource	Source	Identifier
Mouse CD 48, Pac Blue	Biolegend	103418
Mouse/Human CD11b-Biotin	Biolegend	101204
Mouse CD11b, APC-Cy7	BD Biosciences	557657
Mouse CD11c-Biotin	Biolegend	117304
Mouse CD11c, BV510	BD Biosciences	562949
Mouse CD150, Alexa Fluor 647	Biolegend	115918
Mouse CD16/32, PE/Cy7, APC-Cy7	Biolegend, BD Biosciences	101318, 560541
Mouse CD19, BV605	BD Biosciences	563148
Mouse CD206, BV605	Biolegend	141721
Mouse CD3 molecular complex, BV421	BD Biosciences	564008
Mouse CD4-Biotin	Biolegend	100404
Mouse CD45.1, PE-Cy7	Biolegend	110730
Mouse CD45.2, Pac Blue, Alexa Flour 700	Biolegend	109820, 109822
Mouse CD48, Pac Blue	Biolegend	103418
Mouse CD49b (pan NK cells), PE	Biolegend	108908
Mouse CD8a-Biotin	Biolegend	100704
Mouse F4/80, PE-Cy7	Biolegend	123114
Mouse Ly-6G/Ly-6C (Gr1)-Biotin	Biolegend	108404
Mouse IL-7R alpha (CD127) -Biotin	Biolegend	135006
Mouse IL7R alpha (CD127), BV711	BD Biosciences	565490
Mouse Ki-67, BV605	Biolegend	652413
Mouse Ly-6C, PerCP Cy5.5	eBioscience	45-5932-32
Mouse Ly-6G, APC	Biolegend	127614
Mouse MHC-II, Pac Blue, PE-Cy7	Biolegend, eBioscience	107620, 25-5321-82
Mouse NK1.1-Biotin	Biolegend	108704
Mouse NK1.1, PE	Biolegend	108708
Mouse Sca-1, Pac Blue, APC-Cy7	Biolegend	108120, 108126
Mouse Ter119-Biotin	Biolegend	116204
Mouse- c-kit, PerCP	Biolegend	105822
Streptavidin BV605, BV510	BD Biosciences	563260, 563261
Mice		
Adrb1$^{-/-}$ and *Adrb2*$^{-/-}$	JAX	003810
Apoe−/−	JAX	002052
B6GFP	JAX	004353
C57BL/6	JAX	000664
CD45.1	JAX	002014
KikGR	JAX	013753
ROSA 26iDTR	JAX	007900
ROSA tdTOmato	JAX	007914

Reagent or resource	Source	Identifier
Th cre	JAX	025614
Immunofluorescence and Immunoblot antibodies		
Beta-actin	Cell Signaling Technology	4970
CD 3	BD Biosciences	557306
CD 11b	Abcam	Ab133357
CD 45	Sigma Aldrich	SAB4502541
CD 68	eBioscience, Abcam	14-0681-82, ab955
F4/80	Invitrogen	MA1-91124
Ly6G	Biolegend	127602
PGP 9.5	Invitrogen	38-1000
Tyrosine Hydroxylase	Millipore	AB152
Software and algorithms		
Prism 6 and 7	GraphPad	NA
Fiji (Image J)	https://fiji.sc	https://fiji.sc
Imaris	Bitplane	NA
FlowJo	NA	NA

Contact for Reagent and Resource Sharing

Further information and requests for resources and reagents should be directed to and will be fulfilled by the Lead Contact, Partha Dutta (duttapa@pitt.edu).

Experimental model and subject details

Patient samples—Peripheral blood from diabetic patients was collected at Academic Medical Center, Amsterdam, the Netherlands. Diabetes was defined as Hba1c concentrations equal or more than 47 mmol/mol. Blood samples from age-matched patients with Hba1c less than 40 mmol/mol were used as control. After ficol gradient-mediated separation of leukocytes, the cells were stored in 10% DMSO-containing media. Plasma samples and frozen leukocytes were shipped on dry ice to the University of Pittsburgh Medical Center for flow cytometric and catecholamine analysis. Human spleens were collected through a warm autopsy program at the University of Pittsburgh Medical Center under CORID 724.

Mice, diabetes induction and sympathetic ablation

All the strains of mice were obtained from Jackson Laboratories and housed in UPMC Animal Facility in individually ventilated cages and taken veterinary care under the supervision of Division of laboratory animal resources (DLAR). All facilities are USDA registered, covered under an Assurance with the Office of Lab Animal Welfare (OLAW) of the PHS, and accredited by the Association for Assessment and Accreditation of Laboratory Animal Care International (AAALAC). We made all attempts to minimize the number of mice required to complete all the experiments outlined, and all surgeries under anesthesia and administering post-operative analgesics. We used both male and female mice of aged

more than 12 weeks old for all of the experiments. To induce type-1 diabetes, mice were fasted for 6 hours and injected with streptozotocin dissolved in sodium citrate buffer (0.1 mmol/L) pH 4.5 *i.p.*, 22.4 mg/kg/day, for 5 consecutive days. Chemical sympathetic ablation was performed by injecting 6-hydroxydopamine hydrobromide (6-OHDA) through *i.p.*, 250 mg/kg/week, for three weeks.

Method details

Organ harvesting, flow cytometry and cell sorting—Mice were euthenized and perfused thoroughly with 30 ml of ice cold PBS through the left ventricle. The entire aortae were harvested (from the root to the iliac bifurcation), minced into small pieces with a fine scissors and digested in enzymatic mixture containing 450 U/ml collagenase I, 125 U/ml collagenase XI, 60 U/ml DNase I, and 60 U/ml hyaluronidase at 37°C at 750 rpm for 1 h. Cells were passed through 40-μm cell strainer, washed in 10 ml FACS buffer and centrifuged (4°C, 370 g, 7 minutes). Spleens were removed, homogenized in FACS buffer and passed through 70-μm filters, followed by red blood cell lysis in the filtrate. Splenocytes were washed and resuspended in FACS buffer. Total viable cell numbers were obtained from above aliquots using Trypan Blue (Cellgro, Mediatech, Inc, VA). Following harvesting of single cell suspensions, cells were stained in FACS buffer. Cell staining and analysis were performed as described previously (Dutta et al., 2012). All antibodies used in this study were purchased from eBioscience, BioLegend or BD Biosciences. For mature myeloid cells analysis, monoclonal antibodies including anti-CD11b (M1/70), Ly6G (1A8), CD115 (AFS98), Ly6C (AL-21) were used. Neutrophils were identified as CD11b+ Ly6G+, Ly6Clow monocytes were identified as CD11b+ CD115+ Ly6Clow and Ly6Chigh monocytes were defined as CD11b+ CD115+ Ly6Chigh. For hematopoietic stem and progenitor cells analyses, cells were stained with biotin conjugated antibodies against lineage markers including B220 (RA3-6B2), CD4 (GK1.5), CD8a (53-6.7), NK1.1 (PK136), CD11b (M1/70), CD11c (N418), Gr-1 (RB6-8C5), Ter119 (TER-119) followed by streptavidin Pacific OrangeTM or APC/Cy7 conjugates, and antibodies against c- Kit (2B8), Sca-1 (D7), IL7Ra (SB/199), CD93 (AA4.1), CD16/32 (2.4G2), CD34 (RAM34), CD135 (A2F10), CD48 (HM48-1) and CD150 (TC15-12F12.2). Hematopoietic stem cells (HSC) were identified as Lin- c-Kit+ Sca-1+ CD48- CD150+, LKS were identified as Lin- c-Kit+ Sca-1+. Granulocyte-macrophage progenitors (GMP) were identified as Lin- c-Kit+ Sca-1- CD16/32+ CD34+ and macrophage and dendritic cell progenitors (MDP) were defined as Lin- c-Kit+ Sca-1- CD16/32+ CD34+ CD115+. Common lymphoid progenitors (CLP) were identified as Lin- IL7Ra + c-Kit int Sca-1int and early immature B cells were defined as Lin- B220int CD93+. Cell numbers per femur were calculated as total cells per femur sample multiplied by percentage of cells obtained from the appropriate FACS gates. Data acquisition was performed using LSRII Flow Cytometer (BD). Data were analyzed using with FlowJo software (Tree Star).

Treatment with adrenergic β2 receptor antagonist—Following induction of diabetes by stz injection, ICI 118,551 hydrochloride, a selective antagonist of β2 adrenergic receptor (12 μg/kg/hr) was delivered via an osmotic mini pump for 2 weeks.

Treatment with SGLT inhibitor—Following diabetes induction in C57BL/6 wild type mice using stz injection, mice were treated twice daily i.p for two weeks with phlorizin, a competitive inhibitor of SGLT, at a concentration of 200 mg/kg body weight dissolved in 30% DMSO to reduce the blood glucose concentrations.

Catecholamine analysis—To check catecholamine concentrations in sorted macrophages, we cultured the cells at a density of 10,000/well in DMEM medium containing 10 % FBS, non-essential amino acids, penicillin (100 U/mL), streptomycin (100 μg/mL) in the presence or absence of recombinant IL-4 (10 ng/ml). Supernatants were harvested at day 3, and the catecholamines were quantified using epinephrine/ norepinephrine ELISA kit.

Cell sorting, gene expression and heat map analysis—Cells were sorted using a FACS Aria II directly in RNA extraction buffer, total RNA was extracted using ArcturusTM PicoPureTM RNA isolation kit, and cDNA was prepared from 100 ng of mRNA using the high-capacity RNA to cDNA synthesis kit. Quantitative PCR was performed using SYBBR green PCR master mix in Quantstudio 6 Flex Real-time PCR system (Thermo Fisher Scientific), and the results of the indicated genes were expressed as Ct values normalized to the house-keeping gene GAPDH. Heat maps were generated using Microsoft Excel.

Tyrosine hydroxylase (TH) expression

a) Flow cytometry—To check TH expression in splenic leukocytes, we bred the Rosa tdTomato female mice with Th cre male mice to obtain offspring that express tdTomato in TH^+ cells. We analyzed the expression of tdTomato in sorted leukocyte subsets by flow cytometry.

b) Immuno blotting—To check the expression of TH in splenocytes, we sorted the splenocytes from spleen of wild type mice using magnetic activated cell sorting and lysed the cells in 1X RIPA buffer containing proteinase and phosphatase inhibitor cocktail. We also extracted the proteins from whole spleen and brain using 1X RIPA buffer and all the protein lysates were resolved by SDS–PAGE and then blotted onto nitrocellulose membrane using a semidry apparatus (Bio-Rad). Subsequently blots were blocked with 5% BSA in TBST, and incubated with either anti-tyrosine hydroxylase or anti-β-Actin (1:1000 dilution) at 4°C for 18 h. Subsequently blots were incubated with secondary IgG HRP antibody in 0.5% BSA in TBST for 60 minutes and immunoreactive proteins were developed using Luminata Crescendo Western HRP substrate and images were captured by molecular imaging system (ChemiDocTM XRS + System, Bio-Rad).

c) q-PCR—We checked the gene expression of TH in THP1cells that were cultured in 60 mm dishes for 48h in the presence or absence of 50 ng/ml PMA to differentiate monocytes into macrophages. Results were expressed as Ct values normalized to the house-keeping gene GAPDH.

TH^+ leukocyte and neuron depletion—We generated mice expressing iDTR in leukocytes by transplanting bone marrow (BM) from Th-cre-ROSA iDTR mice into wild

type mice. Diabetes was induced in these mice by stz injection. Diptheria toxin (DT) was injected ip. at 10 μg/kg body weight in these mice every other day for a week to deplete the TH^+ leukocytes. Additionally, we generated mice expressing iDTR in neurons by transplanting BM from wild type mice into Th-cre-ROSA iDTR mice. Splenic nerves were depleted in these mice by delivering DT locally into the spleen using micro-osmotic pumps for 7 days.

Catecholamines analysis in cultured macrophages—We enriched macrophages by negative selection using B220, Ter119, Gr1, NK1.1, CD4 and CD8 antibodies. Enriched macrophages were seeded at a density of 20,000 / well in 96 well plates and cultured in the presence or absence of recombinant IL-4 (20 ng/ml). Macrophages were incubated in the presence or absence of various concentrations of reserpine for 3 days and analyzed the concentrations of epinephrine and NE in the conditioned media using ELISA.

Histo-pathological analysis and Immunofluorescence—Aortic root sections were stained with Masson's trichrome to assess plaque size and fibrous cap thickness. For immunohistochemistry, sections were stained with anti-CD11b (clone EPR1344). Following application of appropriate biotinylated secondary antibodies, sections were developed using a Vectastain ABC kit and AEC substrate kit. All sections were counterstained with Harris Hematoxylin and images were taken using a Nikon 90-I microscope. For immunofluorescence staining, tissue sections were permeabilized with 0.1% Triton X-100 for an hour. Mouse tissue sections were stained with anti-CD11b (clone EPR1344), anti-CD3 (clone 145-2C11), anti-F4/80 (clone A3-1), anti-Ly6G (clone 1A8), anti-PGP9.5, anti-CD45 or sheep anti-mouse tyrosine hydroxylase. For tyrosine hydroxylase staining, we used Cy3-labelled donkey anti-sheep secondary antibody. For F4/80 and Ly6G staining, we used Cy5-labelled goat anti-rat secondary antibody. For CD11b, CD3 and PGP9.5 staining, we used Cy5-labelled goat anti-rabbit, Alexa fluor 488-labelled goat anti-hamster, Alexa fluor 488-labelled goat anti-rabbit secondary antibodies respectively. For CD3 and CD68 staining, we used Alexa fluor 488-labelled donkey anti-sheep secondary antibody. The sections were counterstained and fixed with vector shield DAPI, and images were taken using confocal laser scanning immunofluorescence microscopy (CLSM). Image analysis was done using Image J software (Fiji). 3D movies were made with Imaris software (bitplane).

Catecholamine Staining—The glyoxylic acid method described by de la Torre (de la Torre and Surgeon, 1976) was performed. Briefly, 10 μm spleen sections were dipped three times in a sucrose, monobasic potassium phosphate, and glyoxylic acid solution immediately after cutting and dried for 30 min using air from a hair dryer. The excess of dried solution was removed with Kimtech wipers (Kimberly-Clark) to avoid any possible background surrounding the stained tissue. Then, the slides were covered with mineral oil and heated in an oven at 95°C for 3 min, after which excess oil was removed and coverslips were added. Catecholamines were visualized with a Nikon A1 confocal microscope. Auto-fluorescent cells were considered as leukocytes. Image analysis was done using Image J software (Fiji).

BrdU experiments—For BrdU pulse experiments, 1 mg of BrdU was injected i.p twice a day for two weeks. Ten days after the BrdU pulse, the frequency of BrdU-retaining GMP

was determined by flow cytometry. After staining for cell surface antigen, intracellular BrdU staining was performed according to the manufacturer's (BD Bioscience) protocol.

Ultrasound imaging—Transcutaneous ultrasound imaging was performed on the chest using linear array transducer MS 550 (40 MHz) attached to Vevo 2100 (Visualsonics, Toronto, Canada) ultrasound system. Right longitudinal axis parasternal cine loop image of aortic root, ascending aorta, arch of aorta and descending aorta were obtained and stored for offline analysis. Cine loop images were later analyzed using Vevo 2100 software. Intima-media thickness was calculated using previously validated approach(Zhang et al., 2015) i.e. from edge of echo toward the blood stream (intima) to other echo edge (adventitia) using ImageJ (National Institutes of Health).

Splenectomy—Mice were anesthetized using isoflurane (1.5% mixed with oxygen at a flow rate of 2L/minute) and placed on a heating pad to maintain body temperature during the procedure. A sub cutaneous injection of buprenorphine (0.1mg/kg in a volume of 100 μl saline) was administered before the procedure. A laparotomy incision was made, and the spleen, renal vein and renal artery were identified and ligated using a 7-0 silk suture. The vessels were dissected, the spleen was removed and the abdomen was closed in layers using 7-0 suture.

Splenic sympathectomy—After laparotomy incision in the anaesthetized mice splenic nerve was isolated from the splenic blood vessels and connective tissue near the bifurcation of the celiac artery. The entire bundle of the nerve was cut.

Spleen transplantation—After laparotomy incision, renal vein and renal artery were identified and ligated using a 7-0 silk suture. The vessels were dissected, and the spleen was removed. A recipient mouse was also prepared as the donor mice. Laparotomy incision was performed and a part of the donor spleen was transplanted in the renal adipose tissue without vascular anastomosis. Spleens from non-diabetic or diabetic $CD45.1^+$ mice were transplanted in non-diabetic or diabetic $CD45.2^+$ $Apoe^{-/-}$ mice, respectively. Three weeks, after the transplantation, flow cytometry on the blood and aorta was performed to determine donor spleen-derived monocytes. Donor and native spleens were embedded in OCT.

Micro-osmotic pump experiments—$Apoe^{-/-}$ mice (10–12 weeks old) were fed with a high fat diet for 30 days. Afterwards, we induced type-1 diabetes in these mice with stz (*i.p.*, 22.4 mg/kg/day for 5 consecutive days). Micro-osmotic pumps were installed in the spleen of the mice to deliver reserpine (5mg/kg body weight per day), captopril (ACE inhibitor) (6mg/kg body weight per day) or NE (5mg/kg body weight per day) at 0.21 μl/h for 21 days into the spleens. All drugs were dissolved in PBS, and micro-osmotic pumps containing PBS were installed in the control group.

Irradiation and bone marrow transplantation—Mice were placed in the irradiator, non-anesthetized, and performed the irradiation by exposing to 10Gy gamma irradiation for a period of 15 minutes. Then mice were placed in a cage and returned to the housing rooms and injected approximately 1 million bone marrow cells/mouse through i.v under anesthesia.

Statistics—Data are represented as mean±SEM. Statistical significance between groups was performed using Prism *t* test or ANOVA according to the data set. Results were considered as statistically significant when $P<0.05$.

Study approval—All animal experiments were conducted following NIH guidelines under protocols approved by the Institutional Animal care and Use Committee of the University of Pittsburgh. Written informed consent was received from family members of deceased patients before tissue collection for the study.

Supplementary Material

Refer to Web version on PubMed Central for supplementary material.

Acknowledgments

This work was supported by National Institute of Health grants 4R00HL121076-03 and 1R01HL143967 (to PD). The small animal imaging system was supported by NIH 1S10RR027383-01 (to KK). We would like to acknowledge the NIH supported microscopy resources in the Center for Biologic Imaging. Specifically the confocal microscope supported by grant number 1S10OD019973-01. The graphic abstract was adapted from the Servier Medical Art (www.servier.com). We would like to thank Drs. Prabir Ray and Anuradha Ray for their critical review of the manuscript.

References

Andersson U, Tracey KJ. Neural reflexes in inflammation and immunity. J Exp Med. 2012; 209:1057–1068. [PubMed: 22665702]

Barnes MA, Carson MJ, Nair MG. Non-traditional cytokines: How catecholamines and adipokines influence macrophages in immunity, metabolism and the central nervous system. Cytokine. 2015; 72:210–219. [PubMed: 25703786]

Bokhari S, Plummer E, Emmerson P, Gupta A, Meyer C. Glucose counterregulation in advanced type 2 diabetes: effect of beta-adrenergic blockade. Diabetes Care. 2014; 37:3040–3046. [PubMed: 25092686]

Brown SW, Meyers RT, Brennan KM, Rumble JM, Narasimhachari N, Perozzi EF, Ryan JJ, Stewart JK, Fischer-Stenger K. Catecholamines in a macrophage cell line. J Neuroimmunol. 2003; 135:47–55. [PubMed: 12576223]

Carnevale D, Pallante F, Fardella V, Fardella S, Iacobucci R, Federici M, Cifelli G, De Lucia M, Lembo G. The angiogenic factor PlGF mediates a neuroimmune interaction in the spleen to allow the onset of hypertension. Immunity. 2014; 41:737–752. [PubMed: 25517614]

Cortez-Retamozo V, Etzrodt M, Newton A, Rauch PJ, Chudnovskiy A, Berger C, Ryan RJ, Iwamoto Y, Marinelli B, Gorbatov R, et al. Origins of tumor-associated macrophages and neutrophils. Proc Natl Acad Sci U S A. 2012; 109:2491–2496. [PubMed: 22308361]

Dalli J, Colas RA, Arnardottir H, Serhan CN. Vagal Regulation of Group 3 Innate Lymphoid Cells and the Immunoresolvent PCTR1 Controls Infection Resolution. Immunity. 2017; 46:92–105. [PubMed: 28065837]

de la Torre JC, Surgeon JW. Histochemical fluorescence of tissue and brain monoamines: results in 18 minutes using the sucrose-phosphate-glyoxylic acid (SPG) method. Neuroscience. 1976; 1:451–453. [PubMed: 11370236]

DiNicolantonio JJ, Fares H, Niazi AK, Chatterjee S, D'Ascenzo F, Cerrato E, Biondi-Zoccai G, Lavie CJ, Bell DS, O'Keefe JH. beta-Blockers in hypertension, diabetes, heart failure and acute myocardial infarction: a review of the literature. Open Heart. 2015; 2:e000230. [PubMed: 25821584]

Dutta P, Courties G, Wei Y, Leuschner F, Gorbatov R, Robbins CS, Iwamoto Y, Thompson B, Carlson AL, Heidt T, et al. Myocardial infarction accelerates atherosclerosis. Nature. 2012; 487:325–329. [PubMed: 22763456]

Dutta P, Hoyer FF, Grigoryeva LS, Sager HB, Leuschner F, Courties G, Borodovsky A, Novobrantseva T, Ruda VM, Fitzgerald K, et al. Macrophages retain hematopoietic stem cells in the spleen via VCAM-1. J Exp Med. 2015; 212:497–512. [PubMed: 25800955]

Esler M, Rumantir M, Wiesner G, Kaye D, Hastings J, Lambert G. Sympathetic nervous system and insulin resistance: from obesity to diabetes. Am J Hypertens. 2001; 14:304S–309S. [PubMed: 11721888]

Ferraro F, Lymperi S, Mendez-Ferrer S, Saez B, Spencer JA, Yeap BY, Masselli E, Graiani G, Prezioso L, Rizzini EL, et al. Diabetes impairs hematopoietic stem cell mobilization by altering niche function. Sci Transl Med. 2011; 3:104ra101.

Herault A, Binnewies M, Leong S, Calero-Nieto FJ, Zhang SY, Kang YA, Wang X, Pietras EM, Chu SH, Barry-Holson K, et al. Myeloid progenitor cluster formation drives emergency and leukaemic myelopoiesis. Nature. 2017; 544:53–58. [PubMed: 28355185]

Howard BV, Wylie-Rosett J. Sugar and cardiovascular disease: A statement for healthcare professionals from the Committee on Nutrition of the Council on Nutrition, Physical Activity, and Metabolism of the American Heart Association. Circulation. 2002; 106:523–527. [PubMed: 12135957]

Johansson F, Kramer F, Barnhart S, Kanter JE, Vaisar T, Merrill RD, Geng L, Oka K, Chan L, Chait A, et al. Type 1 diabetes promotes disruption of advanced atherosclerotic lesions in LDL receptor-deficient mice. Proc Natl Acad Sci U S A. 2008; 105:2082–2087. [PubMed: 18252823]

Jung WC, Levesque JP, Ruitenberg MJ. It takes nerve to fight back: The significance of neural innervation of the bone marrow and spleen for immune function. Semin Cell Dev Biol. 2016

Kanter JE, Kramer F, Barnhart S, Averill MM, Vivekanandan-Giri A, Vickery T, Li LO, Becker L, Yuan W, Chait A, et al. Diabetes promotes an inflammatory macrophage phenotype and atherosclerosis through acyl-CoA synthetase 1. Proc Natl Acad Sci U S A. 2012; 109:E715–724. [PubMed: 22308341]

Laukova M, Vargovic P, Vlcek M, Lejavova K, Hudecova S, Krizanova O, Kvetnansky R. Catecholamine production is differently regulated in splenic T- and B-cells following stress exposure. Immunobiology. 2013; 218:780–789. [PubMed: 22999161]

Leuschner F, Rauch PJ, Ueno T, Gorbatov R, Marinelli B, Lee WW, Dutta P, Wei Y, Robbins C, Iwamoto Y, et al. Rapid monocyte kinetics in acute myocardial infarction are sustained by extramedullary monocytopoiesis. J Exp Med. 2012; 209:123–137. [PubMed: 22213805]

Libby P. Inflammation in atherosclerosis. Arterioscler Thromb Vasc Biol. 2012; 32:2045–2051. [PubMed: 22895665]

Libby P. Collagenases and cracks in the plaque. J Clin Invest. 2013; 123:3201–3203. [PubMed: 23908120]

Libby P, Ridker PM, Hansson GK. Progress and challenges in translating the biology of atherosclerosis. Nature. 2011; 473:317–325. [PubMed: 21593864]

Muller PA, Koscso B, Rajani GM, Stevanovic K, Berres ML, Hashimoto D, Mortha A, Leboeuf M, Li XM, Mucida D, et al. Crosstalk between muscularis macrophages and enteric neurons regulates gastrointestinal motility. Cell. 2014; 158:300–313. [PubMed: 25036630]

Murphy AJ, Akhtari M, Tolani S, Pagler T, Bijl N, Kuo CL, Wang M, Sanson M, Abramowicz S, Welch C, et al. ApoE regulates hematopoietic stem cell proliferation, monocytosis, and monocyte accumulation in atherosclerotic lesions in mice. J Clin Invest. 2011; 121:4138–4149. [PubMed: 21968112]

Muthu K, Iyer S, He LK, Szilagyi A, Gamelli RL, Shankar R, Jones SB. Murine hematopoietic stem cells and progenitors express adrenergic receptors. J Neuroimmunol. 2007; 186:27–36. [PubMed: 17428548]

Nagareddy PR, Kraakman M, Masters SL, Stirzaker RA, Gorman DJ, Grant RW, Dragoljevic D, Hong ES, Abdel-Latif A, Smyth SS, et al. Adipose tissue macrophages promote myelopoiesis and monocytosis in obesity. Cell Metab. 2014; 19:821–835. [PubMed: 24807222]

Nagareddy PR, Murphy AJ, Stirzaker RA, Hu Y, Yu S, Miller RG, Ramkhelawon B, Distel E, Westerterp M, Huang LS, et al. Hyperglycemia promotes myelopoiesis and impairs the resolution of atherosclerosis. Cell Metab. 2013; 17:695–708. [PubMed: 23663738]

Nguyen KD, Qiu Y, Cui X, Goh YP, Mwangi J, David T, Mukundan L, Brombacher F, Locksley RM, Chawla A. Alternatively activated macrophages produce catecholamines to sustain adaptive thermogenesis. Nature. 2011; 480:104–108. [PubMed: 22101429]

Orlandi A, Chavakis E, Seeger F, Tjwa M, Zeiher AM, Dimmeler S. Long-term diabetes impairs repopulation of hematopoietic progenitor cells and dysregulates the cytokine expression in the bone marrow microenvironment in mice. Basic Res Cardiol. 2010; 105:703–712. [PubMed: 20652278]

Ostman J. beta-adrenergic blockade and diabetes mellitus. A review. Acta Med Scand Suppl. 1983; 672:69–77. [PubMed: 6138937]

Parathath S, Grauer L, Huang LS, Sanson M, Distel E, Goldberg IJ, Fisher EA. Diabetes adversely affects macrophages during atherosclerotic plaque regression in mice. Diabetes. 2011; 60:1759–1769. [PubMed: 21562077]

Renard CB, Kramer F, Johansson F, Lamharzi N, Tannock LR, von Herrath MG, Chait A, Bornfeldt KE. Diabetes and diabetes-associated lipid abnormalities have distinct effects on initiation and progression of atherosclerotic lesions. J Clin Invest. 2004; 114:659–668. [PubMed: 15343384]

Robbins CS, Chudnovskiy A, Rauch PJ, Figueiredo JL, Iwamoto Y, Gorbatov R, Etzrodt M, Weber GF, Ueno T, van Rooijen N, et al. Extramedullary hematopoiesis generates Ly-6C(high) monocytes that infiltrate atherosclerotic lesions. Circulation. 2012; 125:364–374. [PubMed: 22144566]

Rosas-Ballina M, Ochani M, Parrish WR, Ochani K, Harris YT, Huston JM, Chavan S, Tracey KJ. Splenic nerve is required for cholinergic antiinflammatory pathway control of TNF in endotoxemia. Proc Natl Acad Sci U S A. 2008; 105:11008–11013. [PubMed: 18669662]

Rosas-Ballina M, Olofsson PS, Ochani M, Valdes-Ferrer SI, Levine YA, Reardon C, Tusche MW, Pavlov VA, Andersson U, Chavan S, et al. Acetylcholine-synthesizing T cells relay neural signals in a vagus nerve circuit. Science. 2011; 334:98–101. [PubMed: 21921156]

Scheiermann C, Kunisaki Y, Lucas D, Chow A, Jang JE, Zhang D, Hashimoto D, Merad M, Frenette PS. Adrenergic nerves govern circadian leukocyte recruitment to tissues. Immunity. 2012; 37:290–301. [PubMed: 22863835]

Schemann M, Camilleri M. Functions and imaging of mast cell and neural axis of the gut. Gastroenterology. 2013; 144:698–704. e694. [PubMed: 23354018]

Seals DR, Bell C. Chronic sympathetic activation: consequence and cause of age-associated obesity? Diabetes. 2004; 53:276–284. [PubMed: 14747276]

Shankman LS, Gomez D, Cherepanova OA, Salmon M, Alencar GF, Haskins RM, Swiatlowska P, Newman AA, Greene ES, Straub AC, et al. KLF4-dependent phenotypic modulation of smooth muscle cells has a key role in atherosclerotic plaque pathogenesis. Nat Med. 2015; 21:628–637. [PubMed: 25985364]

Spinetti G, Cordella D, Fortunato O, Sangalli E, Losa S, Gotti A, Carnelli F, Rosa F, Riboldi S, Sessa F, et al. Global remodeling of the vascular stem cell niche in bone marrow of diabetic patients: implication of the microRNA-155/FOXO3a signaling pathway. Circ Res. 2013; 112:510–522. [PubMed: 23250986]

Straub RH, Mayer M, Kreutz M, Leeb S, Scholmerich J, Falk W. Neurotransmitters of the sympathetic nerve terminal are powerful chemoattractants for monocytes. J Leukoc Biol. 2000; 67:553–558. [PubMed: 10770289]

Swirski FK, Libby P, Aikawa E, Alcaide P, Luscinskas FW, Weissleder R, Pittet MJ. Ly-6Chi monocytes dominate hypercholesterolemia-associated monocytosis and give rise to macrophages in atheromata. J Clin Invest. 2007; 117:195–205. [PubMed: 17200719]

Swirski FK, Nahrendorf M, Etzrodt M, Wildgruber M, Cortez-Retamozo V, Panizzi P, Figueiredo JL, Kohler RH, Chudnovskiy A, Waterman P, et al. Identification of splenic reservoir monocytes and their deployment to inflammatory sites. Science. 2009; 325:612–616. [PubMed: 19644120]

Tall AR, Yvan-Charvet L. Cholesterol, inflammation and innate immunity. Nat Rev Immunol. 2015; 15:104–116. [PubMed: 25614320]

Thorp AA, Schlaich MP. Relevance of Sympathetic Nervous System Activation in Obesity and Metabolic Syndrome. J Diabetes Res. 2015; 2015:341583. [PubMed: 26064978]

Tracey KJ. Hypertension: an immune disorder? Immunity. 2014; 41:673–674. [PubMed: 25517606]

Trottier MD, Naaz A, Li Y, Fraker PJ. Enhancement of hematopoiesis and lymphopoiesis in diet-induced obese mice. Proc Natl Acad Sci U S A. 2012; 109:7622–7629. [PubMed: 22538809]

Veiga-Fernandes H, Pachnis V. Neuroimmune regulation during intestinal development and homeostasis. Nat Immunol. 2017; 18:116–122. [PubMed: 28092371]

Wang H, Yu M, Ochani M, Amella CA, Tanovic M, Susarla S, Li JH, Wang H, Yang H, Ulloa L, et al. Nicotinic acetylcholine receptor alpha7 subunit is an essential regulator of inflammation. Nature. 2003; 421:384–388. [PubMed: 12508119]

Wendt T, Bucciarelli L, Qu W, Lu Y, Yan SF, Stern DM, Schmidt AM. Receptor for advanced glycation endproducts (RAGE) and vascular inflammation: insights into the pathogenesis of macrovascular complications in diabetes. Curr Atheroscler Rep. 2002; 4:228–237. [PubMed: 11931721]

Westerterp M, Gourion-Arsiquaud S, Murphy AJ, Shih A, Cremers S, Levine RL, Tall AR, Yvan-Charvet L. Regulation of hematopoietic stem and progenitor cell mobilization by cholesterol efflux pathways. Cell Stem Cell. 2012; 11:195–206. [PubMed: 22862945]

Zhang X, Ha S, Wei W, Duan S, Shi Y, Yang Y. Noninvasive imaging of aortic atherosclerosis by ultrasound biomicroscopy in a mouse model. J Ultrasound Med. 2015; 34:111–116. [PubMed: 25542946]

HIGHLIGHTS

1. Sympathetic nervous system (SNS) mediates differentiation of myeloid progenitors.
2. TH^+ leukocytes express high amounts of neuropeptide Y receptors (NPYR).
3. TH^+ cells are required for myeloid cell generation during “emergency” hematopoiesis.
4. Regulation of myelopoiesis by the β_2 adrenergic receptor expressed by GMP.

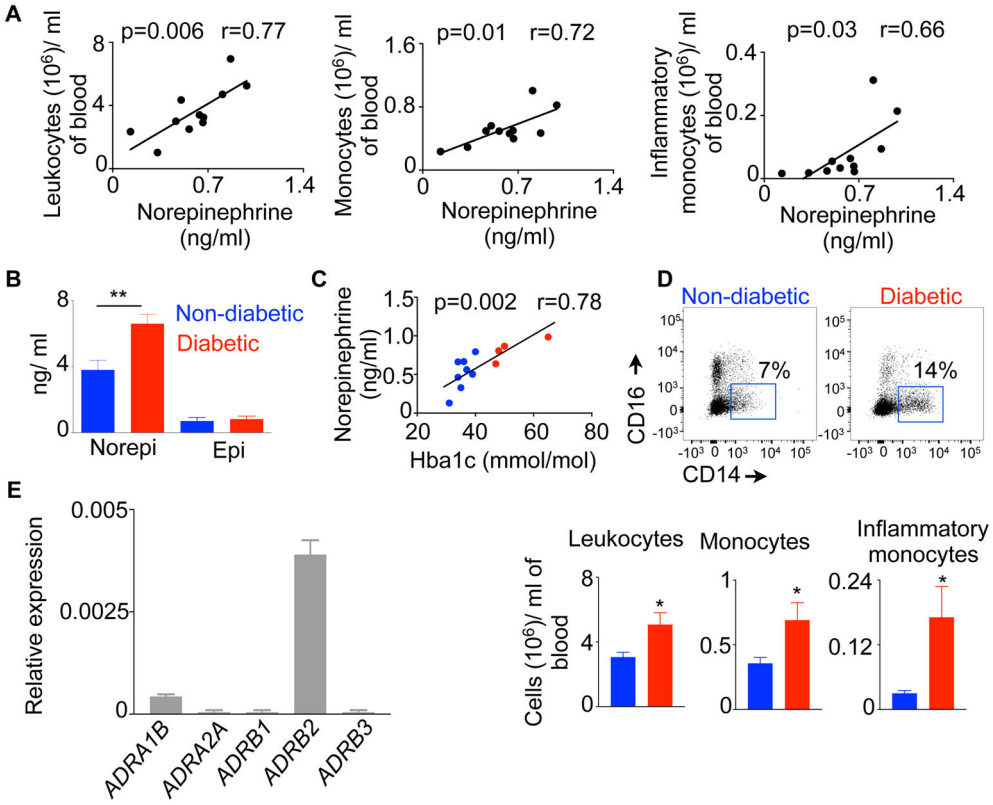

Fig. 1. Plasma Norepinephrine (NE) concentrations strongly correlate with circulatory myeloid cell numbers in patients

A) Plasma NE concentrations are correlated with circulatory leukocyte, monocyte and inflammatory monocytes in patients. **B)** Catecholamine concentrations in diabetic patients. **C)** Correlation between NE and Hba1c in patients. **D)** Circulatory leukocyte, monocyte and inflammatory monocyte numbers determined by flow cytometry. **E)** Relative expression of the adrenergic receptors in GMP isolated from human spleens. n=4–8/group. Mean ± s.e.m. * $P < 0.05$, ** $P < 0.01$.

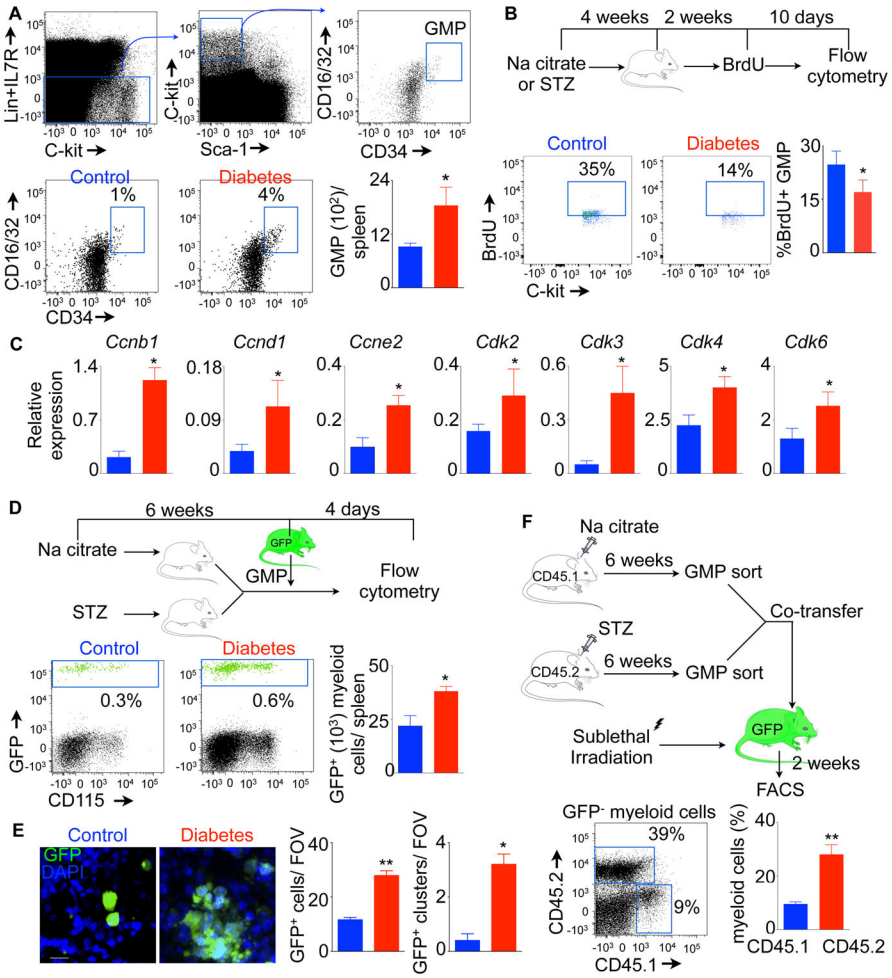

Fig. 2. Splenic GMP proliferate and differentiate into myeloid cells in diabetic C57BL/6 mice

A) Shows representative flow cytometric gating strategy and quantification of splenic GMP. **B**) Quantification of BrdU$^+$ GMP at the end of 10 days of chase after BrdU saturation. **C**) Quantitation of cell cycle regulating genes in splenic GMP using quantitative RT-PCR. Enumeration of donor-derived myeloid cells in the spleen after GFP$^+$ GMP transfer in diabetic and non-diabetic control mice using flow cytometry (**D**) and confocal microscopy (**E**). Scale bar = 10 μm. **F**) Quantification of donor GMP-derived myeloid cells in sublethally irradiated mice. With an exception of Fig. 2F, all data are pooled from at least two independently performed experiments. n=10/group (A) and n=5–6 mice/group (B–F). Mean ± s.e.m. * $P < 0.05$, ** $P < 0.01$. Please also see Figure S1.

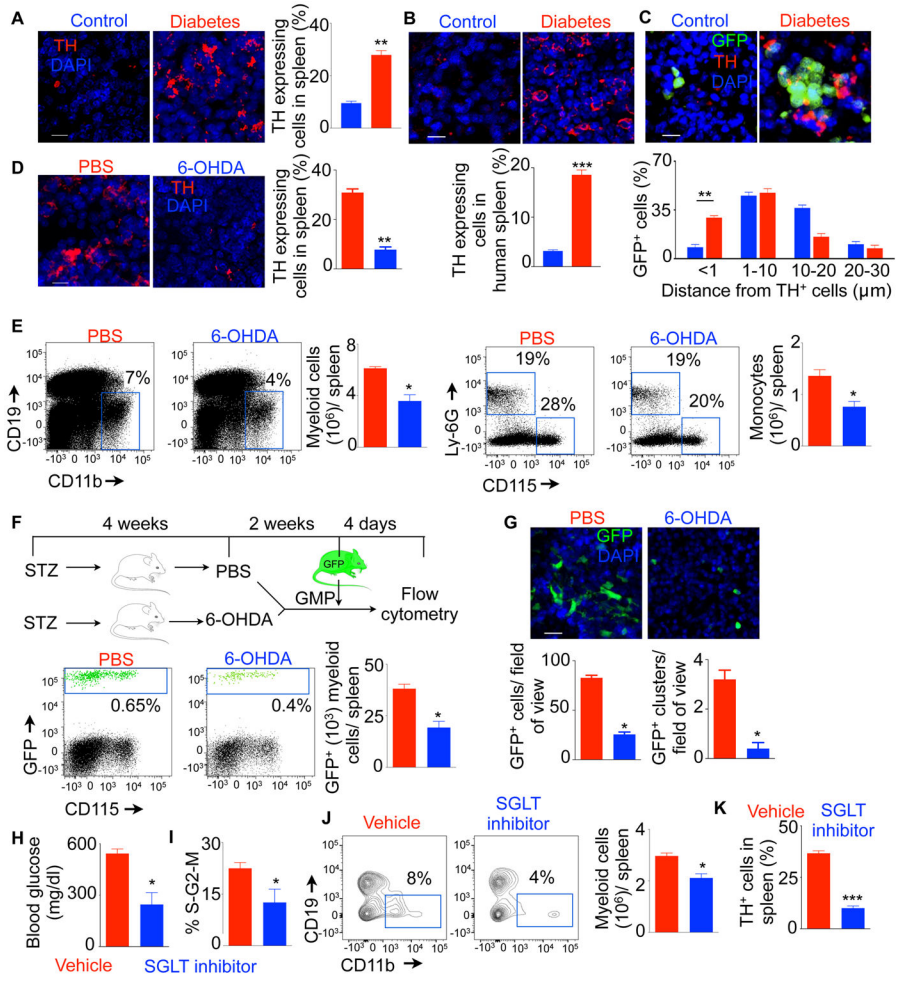

Fig. 3. Splenic myelopoiesis is regulated by sympathetic neuronal activity in diabetic C57BL/6 mice

Immunofluorescent confocal images and quantification of tyrosine hydroxylase $(TH)^+$ cells in the spleen of control and diabetic C57BL/6 mice (**A**) (Scale bar = 20 μm.) and humans (**B**) (Scale bar = 10 μm.). **C**) Measurement of distances between GFP^+ splenocytes derived from transferred GMP and TH^+ cells in the spleen. Scale bar = 10 μm. **D**) TH-stained cells in the spleen after 6-OHDA treatment. Scale bar = 20 μm. **E**) Representative flow cytometric plots and bar graphs showing quantification of myeloid cells after 6-OHDA treatment in the diabetic mice. Quantification of donor GMP-derived GFP^+ myeloid cells after 6-OHDA treatment by flow cytometry (**F**) and confocal microscopy (**G**) (Scale bar = 20 μm). **H**) Fasting blood glucose concentrations after SGLT inhibitor treatment. Flow cytometric analysis for GMP proliferation (**I**) and myeloid cell enumeration (**J**). **K**) The frequency of TH-expressing splenic leukocytes was determined using confocal microscopy. All data except H–K are pooled from at least two independently performed experiments. n=8/ group (A–C), n=10/ group (D), n=6/ group (E–G) and n=4 / group (H–K). Mean ± s.e.m. * $P < 0.05$, ** $P < 0.01$, *** $P < 0.001$.

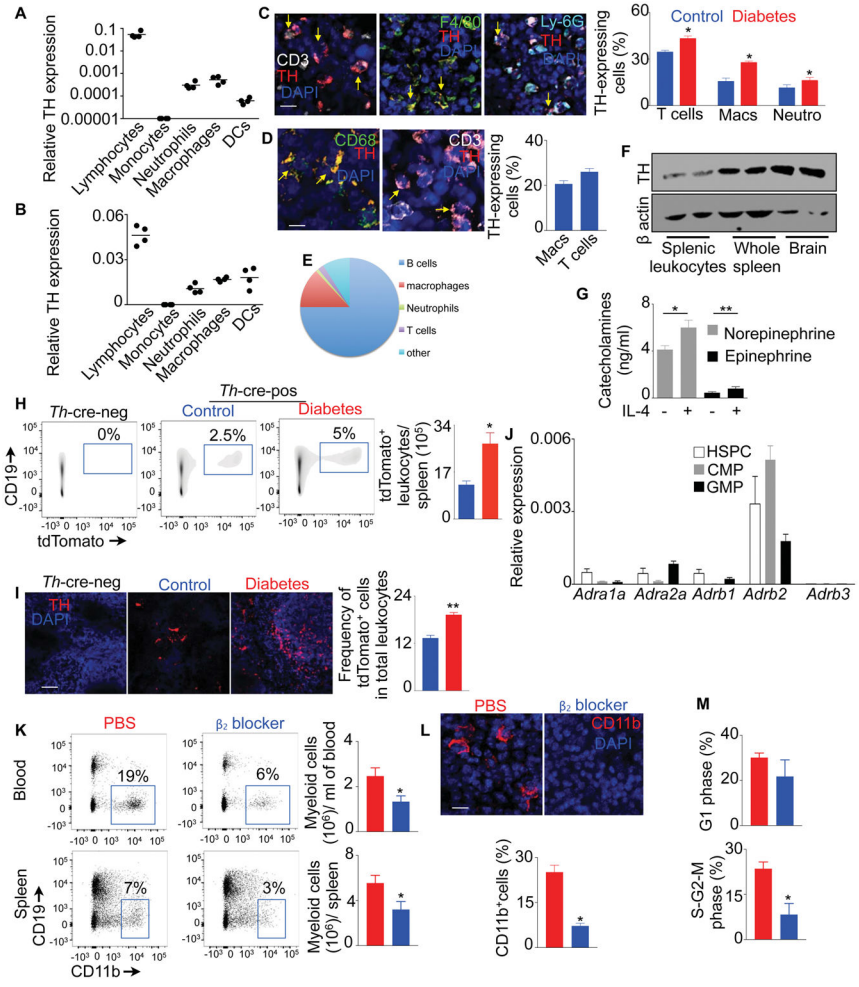

Fig. 4. β_2 adrenergic receptor blockade reduces splenic myelopoiesis

Quantitation of TH expression by lymphocytes ($CD11b^-$ $CD3^+$ or $CD19^+$), monocytes ($CD3^-$ $CD19^-$ $CD11b^+$ $CD115^+$ $Ly\text{-}6G^-$), neutrophils ($CD3^-$ $CD19^-$ $CD11b^+$ $CD115^-$ $Ly\text{-}6G^+$), macrophages ($CD3^-$ $CD19^-$ $F4/80^+$ $CD64^+$) and DCs ($CD3^-$ $CD19^-$ $F4/80^-$ $CD11c^+$) sorted from the spleens of non-diabetic C57BL/6 mice (**A**) and humans (**B**) using quantitative RT-PCR. Please also see Figure S2. Quantification of TH-expressing splenic T cells, macrophages and neutrophils in mouse (**C**) (Scale bar = 10 μm) and human (**D**) (Scale bar = 10 μm) spleens by confocal microscopy. **E**) Distribution of TH-$tdTomato^+$ cells among various leukocyte population in non-diabetic *Th*-cre-ROSA-tdTOmato mice. Please also see Figure S3. **F**) Immuno blot to detect TH in sorted splenic leukocytes, whole spleen and brain of non-diabetic wild type mice. **G**) Catecholamine production by splenic macrophages in culture in the presence or absence of IL-4. Quantification of $tdTomato^+$ leukocytes in *Th*-cre-ROSA-tdTOmato mice by flow cytometry (**H**) and immunofluorescence (**I**) (Scale bar = 100 μm). **J**) Quantification of mRNA amounts of the adrenergic receptors expressed by splenic hematopoietic progenitors sorted from non-diabetic mice using quantitative RT-PCR. **K**) Flow cytometric enumeration of myelo cells in the blood and spleen after β_2 blocker treatment in diabetic mice. **L**) Confocal images and quantification of myeloid cells in the spleen after β_2 blocker treatment in diabetic mice (Scale bar = 10 μm). **M**) Flow cytometric

analysis of the cell cycle of GMP after β_2 blocker treatment in diabetic mice. All data except Fig. 4B are pooled from two independently performed experiments. n=4/ group (A–D), n=2/ group (F), n=7/group (E, H & I), n=5/ group (G) and n=9–10/ group (K–M). Mean ± s.e.m. * $P < 0.05$, ** $P < 0.01$.

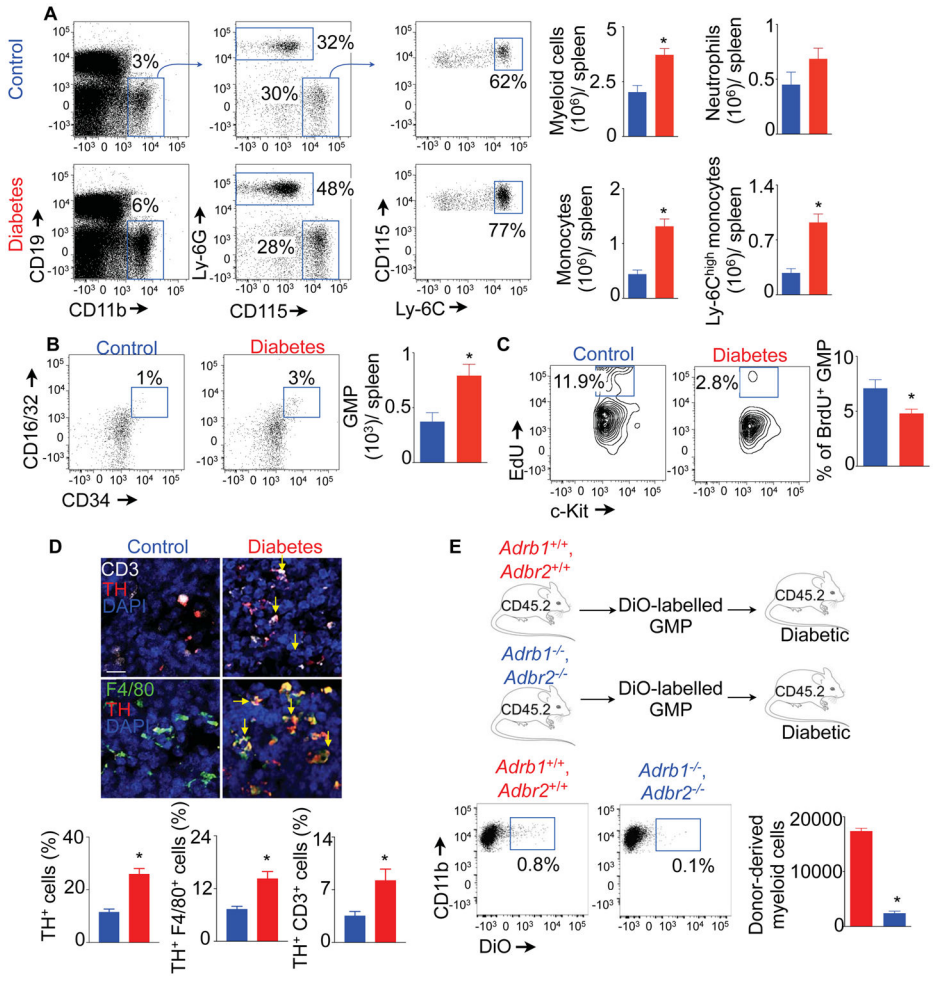

Fig. 5. Sympathetic neuronal activation triggers myelopoiesis in type 2 diabetes

C57BL/6 mice were fed with a high fat diet for 16 weeks. **A**) Flow cytometric enumeration of myeloid cells in the spleens. **B**) Quantification of splenic GMP. **C**) Measurement of GMP proliferation with a BrdU dilution assay. **D**) Quantification of TH^+ leukocytes, macrophages and T cells in the spleen. (Scale bar = 10 μm). **E**) Schematic representation of the experimental design and quantification of donor GMP-derived myeloid cells. All of the experiments were performed at least twice. n=8/ group (A&B) and n=8–12 mice/ group (C–E). Mean ± s.e.m. * $P < 0.05$, ** $P < 0.01$. See also Figure S6.

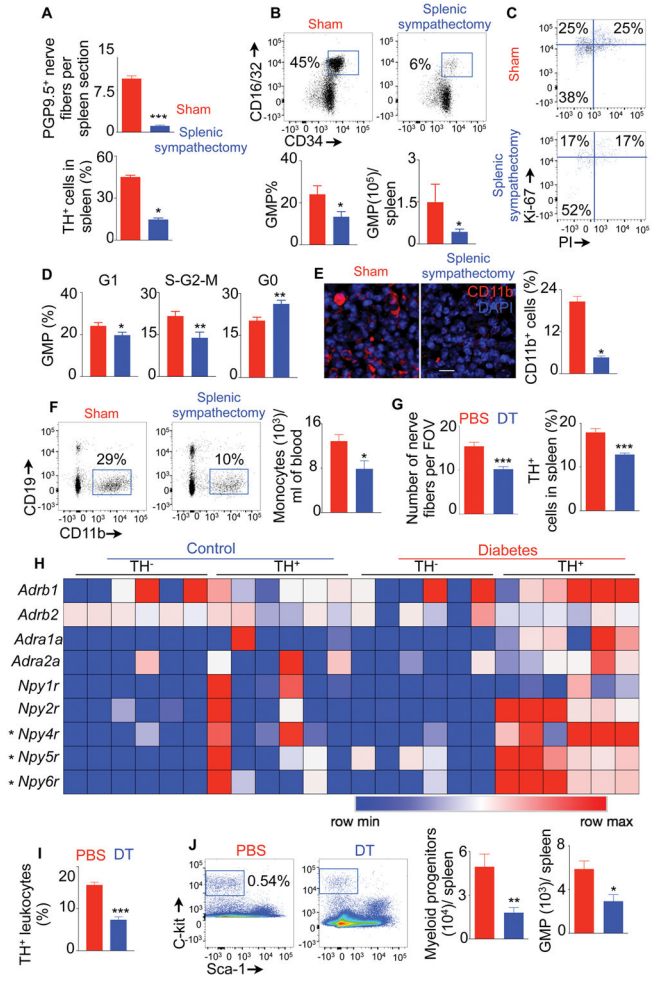

Fig. 6. Splenic sympathectomy and TH$^+$ leukocyte depletion diminish diabetes-induced splenic myelopoiesis

Quantification of splenic PGP9.5$^+$ nerve fibers and TH-expressing cells (**A**), enumeration of splenic GMP (**B**) and cell cycle analysis of splenic GMP (**C&D**) after surgical splenic sympathectomy. **E**) Confocal images and quantification of CD11b$^+$ myeloid cells in the spleen after surgical splenic sympathectomy. (Scale bar = 10 μm). **F**) Quantification of monocytes in the blood using flow cytometry. Scale bar = 10 μm**. G**) Quantification of splenic nerve termini and TH-expressing leukocytes in the spleen after DT injection in *Th*-cre-ROSA-iDTR mice transplanted with wild type BM cells. **H**) Adrenergic receptors and neuropeptide Y (NPY) receptors were quantified by PCR array in TH$^+$ and TH$^-$ cells isolated from the spleens of non-diabetic and diabetic *Th*-cre-ROSA-tdTomato mice. **I**) Quantification of TH$^+$ splenic leukocytes after DT injection in wild type mice reconstituted with BM from *Th*-cre-ROSA-iDTR. **J**) Myeloid progenitor and GMP numbers in the spleen determined by flow cytometry after TH$^+$ leukocyte depletion. All data are pooled from at least two independently performed experiments. n=8–9/group (A–D), n=8/group (E–G) and n=6–7 mice/ group (H–J). Mean ± s.e.m. *$P < 0.05$, ** $P < 0.01$, *** $P < 0.001$. Please also see Figure S4.

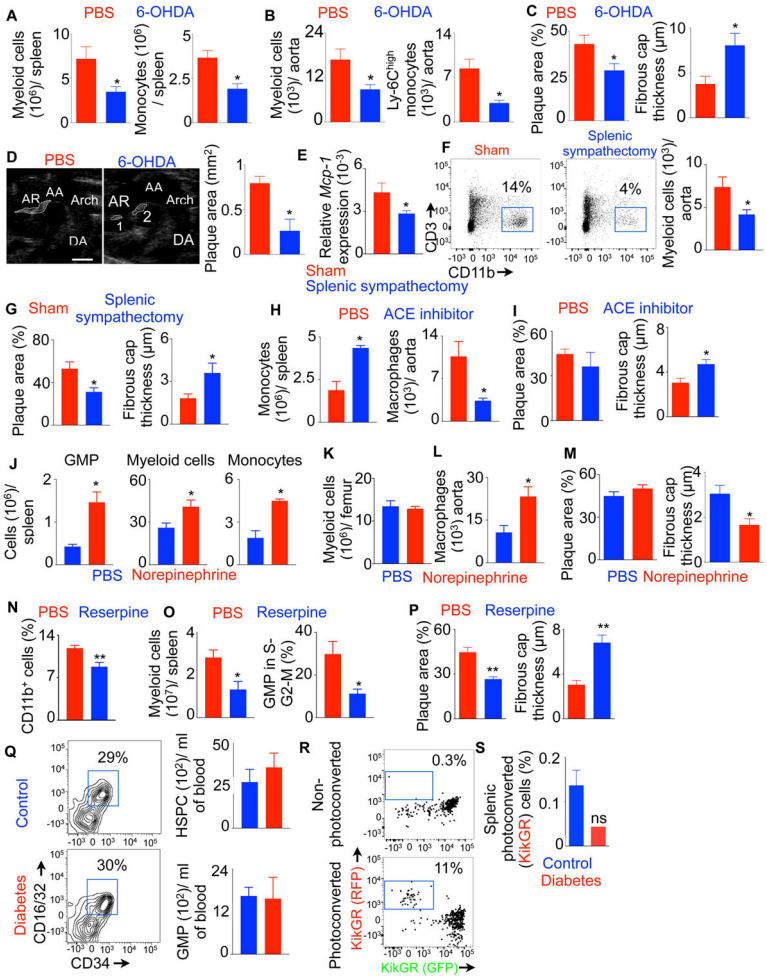

Fig. 7. Sympathetic neuronal activation in diabetes accelerates atherosclerosis

A) Flow cytometric quantification of splenic myeloid cells in diabetic *Apoe*$^{-/-}$ mice after 6-OHDA treatment**. B**) The bar graphs depict quantification of myeloid cells in the aorta. **C**) Quantification of atherosclerotic plaque area and fibrous cap thickness by Masson's trichrome staining. **D**) Representative ultrasound images showing plaques in the aortic root. The bar graph shows quantification of atherosclerotic plaque area. (Scale bar = 1 mm). **E**) Relative Mcp-1 expression in the aorta of diabetic *Apoe*$^{-/-}$ mice after sham surgery or splenic sympathectomy. Enumeration of myeloid cells in the aortas (**F**) and histological analysis of atherosclerotic plaques (**G**) of *Apoe*$^{-/-}$ mice at 4 weeks after splenic sympathectomy. ACE inhibitor, NE, reserpine or PBS was administered into the spleens of diabetic *Apoe*$^{-/-}$ mice using micro-osmotic pumps for three weeks. **H–P**) Myeloid cells in the spleen, BM and aorta were enumerated by flow cytometry. Atherosclerotic plaque area and fibrous cap thickness were quantified using Masson's trichrome staining. n=5 per group. **Q**) Hematopoietic progenitors in the blood were quantified in non-diabetic (control) and diabetic mice. n=4 per group. **R**) Representative flow cytometric plots showing photoconverted cells in the calvarium of KikGR mice. **S**) Enumeration of the photoconverted cells in the spleen. n=3–11 per group. n=6–8/ group (A,B,C), n=8–9/ group (D–G), n=4–5/

group (H–Q) and n=3–11 mice/ group (R&S). Mean ± s.e.m. * $P < 0.05$, ** $P < 0.01$. Please also see Figures S5–7.